Timely Issues

Satellite Signatures in SLR Observations

G.M. Appleby
Royal Greenwich Observatory
Madingley Road
Cambridge CB3 0EZ, UK

Abstract.

We examine the evidence for the detection of satellite-dependent signatures in the laser range observations obtained by the UK single-photon SLR system. Models of the expected observation distributions from Ajisai and Lageos are developed from the published satellite spread functions and from the characteristics of the SLR system, and compared with the observations. The effects of varying return strengths are discused using the models and by experimental observations of Ajisai, during which a range of return levels from single to multiple-photons is achieved. The implications of these results for system-dependent centre of mass corrections are discussed.

1. Introduction.

The UK SLR system sited at Herstmonceux, and run by the Royal Greenwich Observatory, routinely observes the primary targets ERS-1, Lageos, Etalon-1 and -2, Starlette and Ajisai. The single-shot precision achieved by calibration ranging is close to 1 cm (1-sigma). The detection and timing hardware has recently been upgraded to include a Single Photon Avalanche Photodiode (SPAD, Prochazka et al, 1990), and an HP 5370 time interval counter. Epoch is derived at present from a Maryland 4-stop event timer, which is also used to make range measurements simultaneously and independently of the HP counter. Pass-averaged return rates are in general fairly low, varying from a few percent from the Etalon satellites, through about 20% from Lageos to up to 50% from Ajisai. Returns from the calibration targets are deliberately kept to similarly low levels (about 10-15%) using neutral density filters in the laser path. Under such conditions we can describe the system as a single photon return, single photon detection system. A detailed study of the system error budget was carried out following the upgrade of the detector from a PMT. During this investigation it became clear that the observational precision of in particular Lageos and Ajisai was consistently worse than that of the calibration targets. It was considered likely that the spacial distribution of the retroreflector arrays on the satellites would modify the distribution of the range residuals, when compared with those from the flat calibration targets. In this paper we examine the evidence for detection of satellite signatures in our range observations, compare the observations with models of the expected distributions from a selection of those satellites regularly observed, and discuss the implications in terms of the appropriate corrections required to reduce the observations to the centres of mass of the satellites

2. Observations.

This investigation is based upon the pass-by-pass range residuals that are formed during

the preprocessing stage to compute on-site normal points. All trends in the residuals due to errors in the predicted orbit of the satellite are removed during this process, which iteratively solves for corrections to a set of orbit-related parameters, rejecting at each stage residuals falling outside a 3-sigma band (Appleby and Sinclair, 1992, these proceedings). In a final stage of pre-processing, and as a useful check on system performance, the residuals are used to form a frequency distribution for each pass, by grouping the residuals in range bins. A normal distribution is fitted to the observed distribution by iterative least-squares, and the parameters of the fitted Gaussian are used to make a final selection of the original observations. Examples of the observed distributions and their fitted Gaussian distributions are shown in Figure 1. Also shown in the Figure is a typical distribution of ranges to a calibration target board, distant about 600 m from the SLR system. The observed range values are plotted relative to the mean of the fitted Gaussian distributions, which are also shown on each plot. The standard deviations of the fitted distributions are shown, along with higher moments of the data, expressed as skewness and kurtosis. For a perfect Gaussian distribution the values of skewness and kurtosis would be 0.0 and 3.0 respectively.

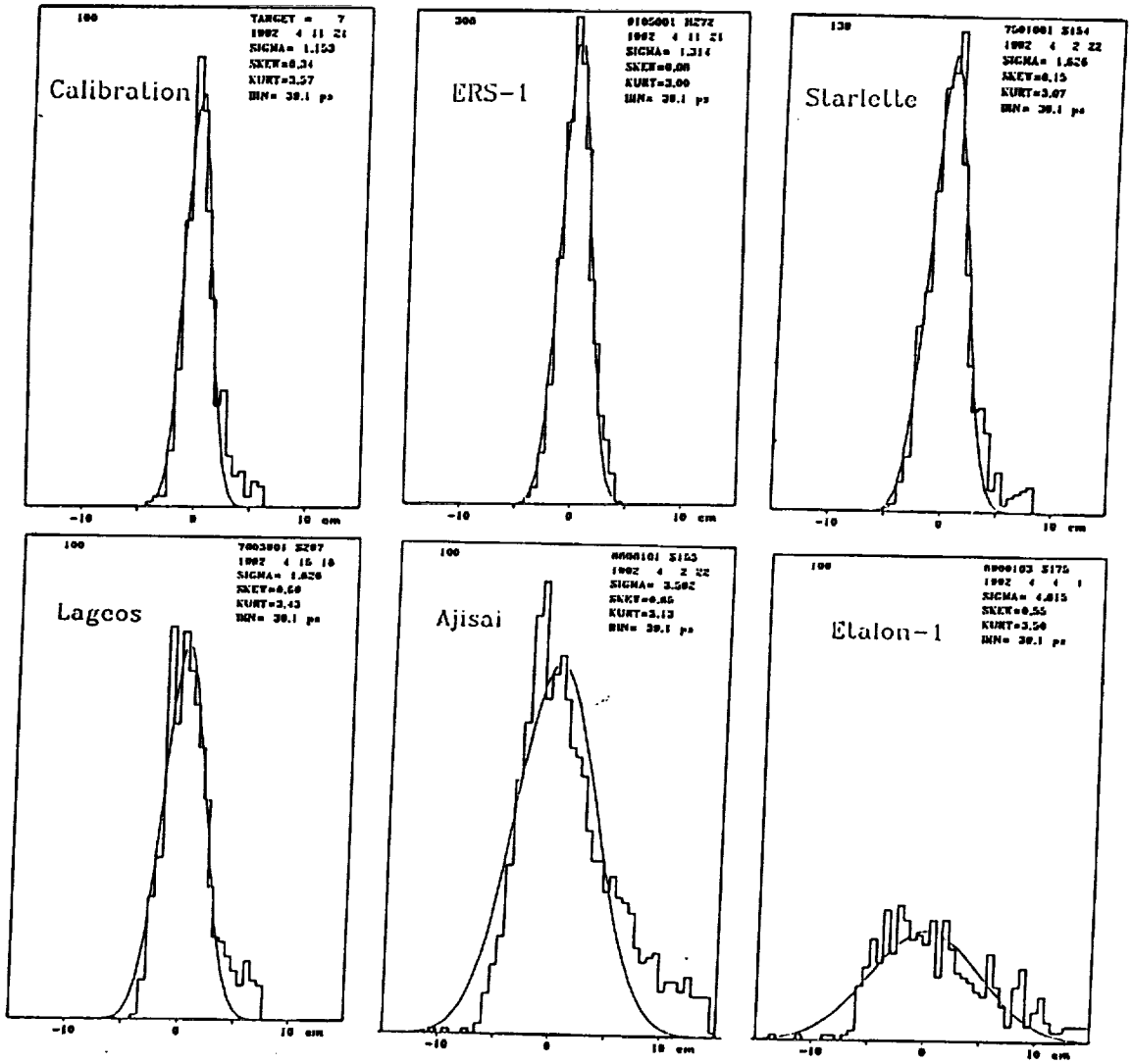

Figure 1. Observed distributions of range residuals from calibration and satellite targets.

2.1 Discussion.

From the distributions shown in Figure 1, we make the following observations. The distributions of the calibration ranges and those from Starlette and ERS-1 are clearly symmetric and well-fitted by the Gaussian distributions, but all have a significant 'tail' of observations outside the fitted curves. Skewness values for these 3 targets are between 0.05 and 0.1. The Lageos distribution is much less symmetric, and is less well fit by the Gaussian distribution. A chi-square goodness of fit test indicates significant departure, at a 5% level of significance, from the best-fit distribution shown in the plot. The results from Ajisai and Etalon 1 show large asymmetry, and are not at all well fit by the Gaussian distributions. Of particular significance to this investigation, are the 'widths' of the distributions, characterized by the standard deviations of the fitted distributions. Mean values of these standard deviations for a number of observations made during November and December 1991 are given in the Table below. These mean values of standard deviations confirm the impression given in Figure 1, that the calibration ranges have the smallest scatter, and those of Ajisai and Etalon-1 the largest, the range of standard deviations being from 1.1 cm to 4.8 cm.

Target	σ
	mm
Calib	11
ERS-1	12
Starlette	16
LAGEOS	18
Ajisai	32
Etalon	48

Before proceeding to investigate the hypothesis that satellite signatures are present in our observations, we first consider the possible causes of the 'tail' in the distributions, particularly evident in the calibration and Starlette data. We remark here that the existence of this tail does not constitute the thrust of our argument that we are detecting satellite signatures in our observations, since the tail is also present in the calibration ranges from a flat target board. We must therefore rule out such a target-induced effect and consider as probable cause the SPAD or the laser. In an experiment primarily designed to quantify the system time-walk under a large range of return signal strengths, calibration ranging was carried out using neutral density filters to vary the average number of photons reaching the detector. In this way the average number of photons was varied from about 0.5 to 50 photons per shot, as deduced from the observed return rates. A selection of the results is given in Figure 2, where the results are displayed in histogram form as before. The plots show, as expected, a reduction in the standard deviations of the distributions with increasing signal strength, since for a given laser pulse-width we would expect the contribution of the laser to the observational jitter to decrease with increasing number of photons in the return train, as the single-event detector increasingly receives photons originating nearer to the leading edge of the transmitted pulse. The plots also demonstrate that the extent of the tail in the distributions decreases with signal strength, suggesting an origin within the laser. However Prochazka (1992, private communication), points out that correct optical alignment

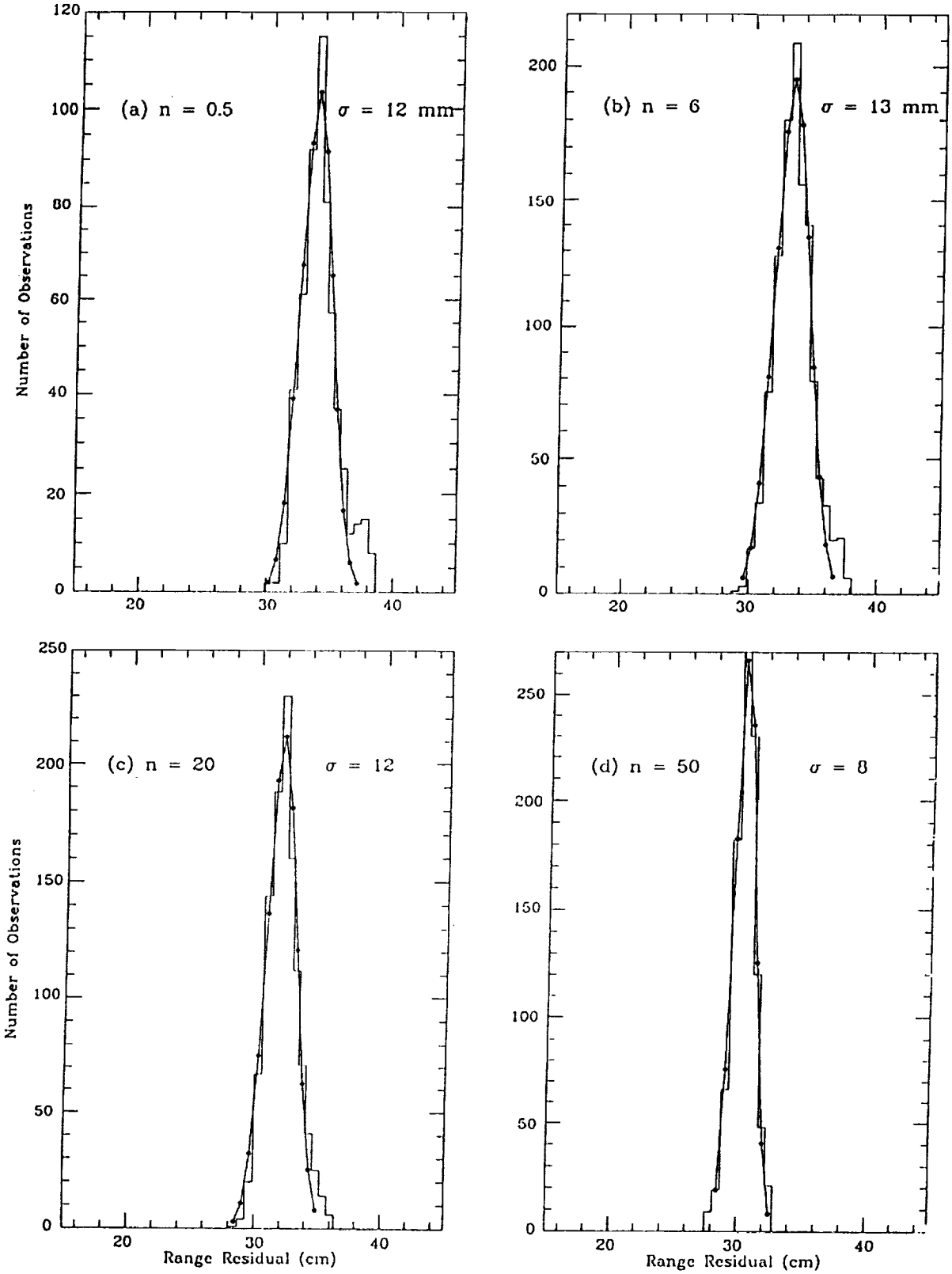

Figure 2. Calibration distributions as a function of average numbers n of returning photons.

of the SPAD detector is essential to avoid possible effects of non-uniformity within the chip. Resolution of this problem awaits further experimentation.

3. Satellite Signature Models.

We now take as our standard, single-photon system-signature the calibration distribution shown in Figure 1, and develop from it models of expected satellite return signatures, by convolution with the spread functions of Lageos and Ajisai. For Lageos, we take the model of cross-section parameters based upon row-by-row far-field diffraction pattern tests in polar orientation, presented in Fitzmaurice *et al* (1977). The parameters give, for the particular orientation, the lidar cross-section and number of corner cubes, in rows, contributing to the strength of returning signal. Also given is the optical distance of each row of reflectors from the spacecraft centre of gravity. We use the effective cross section of the cubes in their rings, of known distances from the centre of the satellite, to carry out a convolution of our system signature with that of Lageos. In this estimate of the shape of the returning pulse we ignore the effects of changing polarisation, which mainly affects the amplitude of the convolved pulse, and not its shape (Fitzmaurice *et al* 1977.) To model the return signatures from Ajisai we use the results of a computer simulation carried out by Sasaki and Hashimoto (1987). They find that the number of retroreflector sets contributing to the return signal from a given single laser pulse can only be 1, 2 or 3.5, and give the computed pulse shape in each of these 3 cases. The laser used in their simulation is gaussian in profile, of standard deviation 33 ps. From the published profiles, we can infer the spread distributions, consisting of lidar cross-sections and distances from spacecraft centre of gravity. We now have the information required to carry out a convolution with our system signature, in the same way as for Lageos. We assume that the rapid spin rate of Ajisai, of 40 rpm (Sasaki and Hashimoto, 1987) will ensure that for every pass all 3 possible orientations of the satellite will be sampled. We thus convolve our system signature with each of the spread distributions, and sum the resulting 3 distributions.

The results of the simulations for Lageos and Ajisai are shown in histogram form in Figures 3(a) and (b), where the quoted standard deviations are those of the fitted Gaussian distributions, also shown on the plots. For completeness we also present in Figure 3 the result of convolving our system separately with each of the 3 orientations of Ajisai.

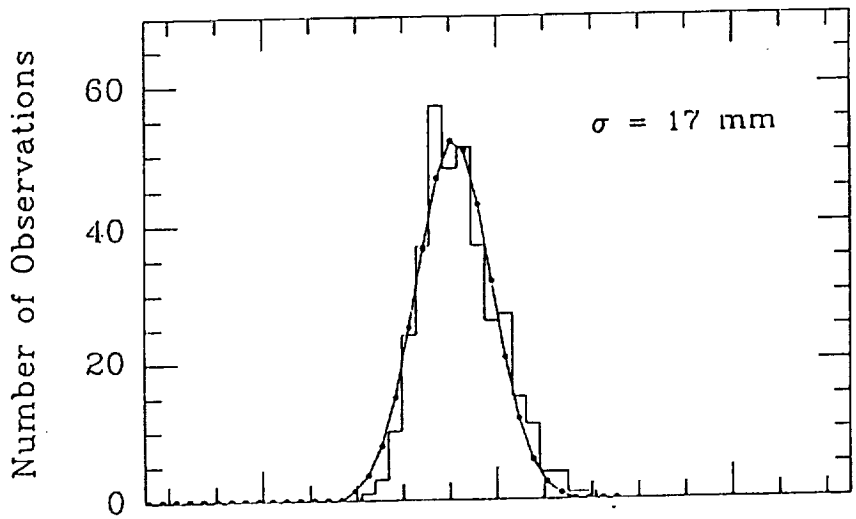

Figure 3. (a) Simulated Lageos range residual distributions.

of the SPAD detector is essential to avoid possible effects of non-uniformity within the chip. Resolution of this problem awaits further experimentation.

3. Satellite Signature Models.

We now take as our standard, single-photon system-signature the calibration distribution shown in Figure 1, and develop from it models of expected satellite return signatures, by convolution with the spread functions of Lageos and Ajisai. For Lageos, we take the model of cross-section parameters based upon row-by-row far-field diffraction pattern tests in polar orientation, presented in Fitzmaurice *et al* (1977). The parameters give, for the particular orientation, the lidar cross-section and number of corner cubes, in rows, contributing to the strength of returning signal. Also given is the optical distance of each row of reflectors from the spacecraft centre of gravity. We use the effective cross section of the cubes in their rings, of known distances from the centre of the satellite, to carry out a convolution of our system signature with that of Lageos. In this estimate of the shape of the returning pulse we ignore the effects of changing polarisation, which mainly affects the amplitude of the convolved pulse, and not its shape (Fitzmaurice *et al* 1977.) To model the return signatures from Ajisai we use the results of a computer simulation carried out by Sasaki and Hashimoto (1987). They find that the number of retroreflector sets contributing to the return signal from a given single laser pulse can only be 1, 2 or 3.5, and give the computed pulse shape in each of these 3 cases. The laser used in their simulation is gaussian in profile, of standard deviation 33 ps. From the published profiles, we can infer the spread distributions, consisting of lidar cross-sections and distances from spacecraft centre of gravity. We now have the information required to carry out a convolution with our system signature, in the same way as for Lageos. We assume that the rapid spin rate of Ajisai, of 40 rpm (Sasaki and Hashimoto, 1987) will ensure that for every pass all 3 possible orientations of the satellite will be sampled. We thus convolve our system signature with each of the spread distributions, and sum the resulting 3 distributions.

The results of the simulations for Lageos and Ajisai are shown in histogram form in Figures 3(a) and (b), where the quoted standard deviations are those of the fitted Gaussian distributions, also shown on the plots. For completeness we also present in Figure 3 the result of convolving our system separately with each of the 3 orientations of Ajisai.

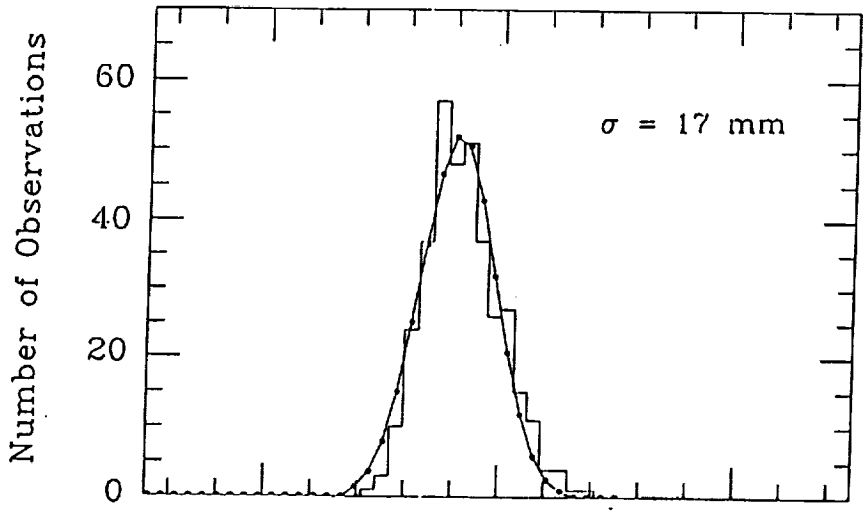

Figure 3. (a) Simulated Lageos range residual distribution

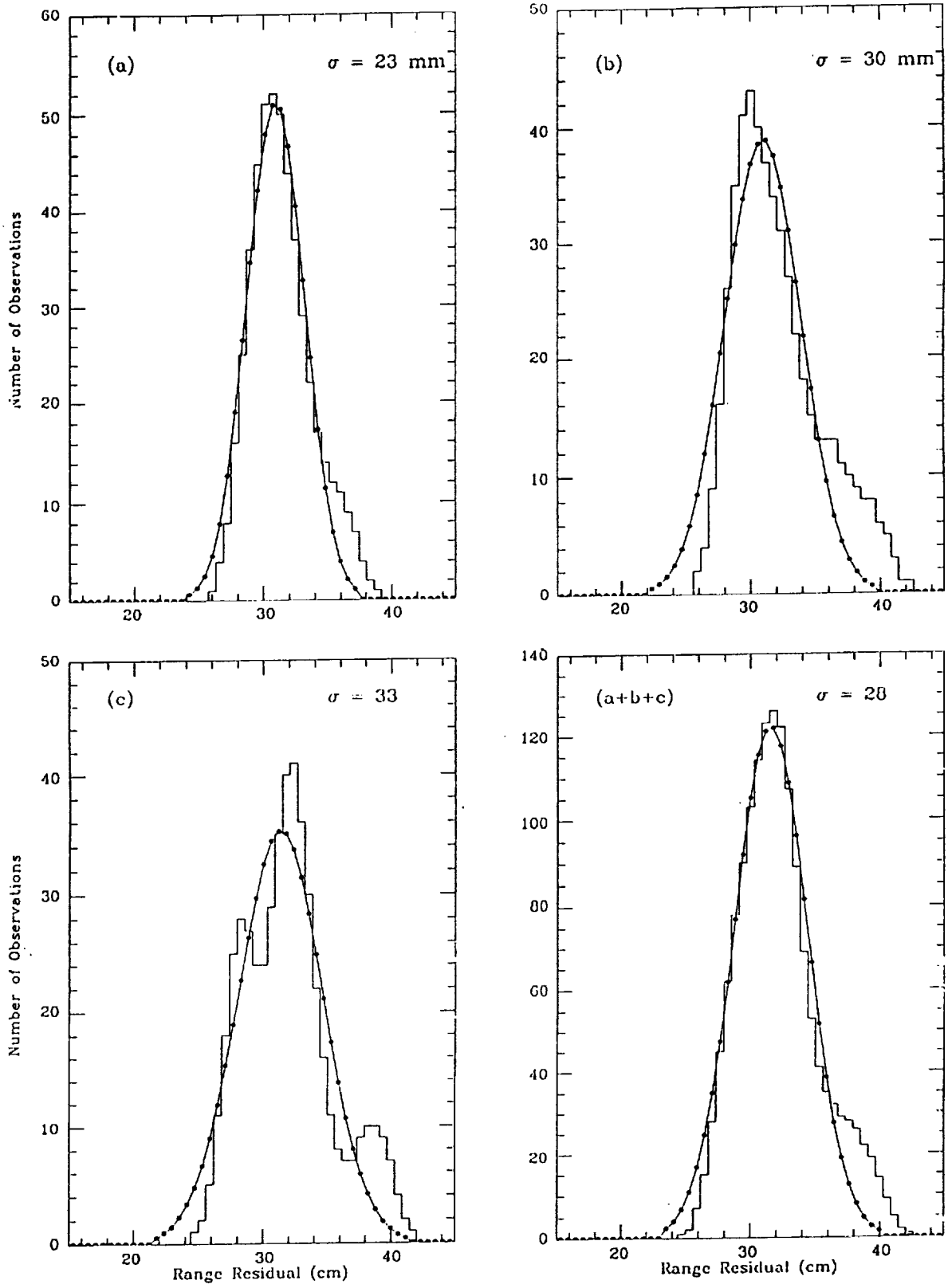

Figure 3. (b) Simulated Ajisai range residual distributions.

3.1 Discussion.

The standard deviation of the simulated Lageos data (1.7 cm) is close to our observational mean of 1.8 cm, and the appearance of the simulated and observed histograms is similar. The underestimate of the observed scatter by our model may be attributed to various causes; neglect of atmospheric turbulence (Gardner, 1976); neglect of coherency fading induced by the satellite, and the single satellite orientation chosen for the model. The models of the Ajisai return signatures give standard deviations of between 2.3 and 3.3 cm, which compare well with the observational results. There is some evidence in the Ajisai observations of variations of signature with pass circumstances, which may be due to the dominance of a particular satellite orientation or orientations for a given ground track.

4. Multi-photon Returns.

The foregoing discussion is based upon return energies at the single photon level; the detected photon is considered to be a random event taken from a population formed by the convolution of the laser pulse distribution with that of the satellite response. We now consider the effects of a larger number of photons reaching the single-photon detector, in order to quantify the subsequent systematic effects caused by a signal-strength-dependent variation of the mean reflection distance to the satellite.

4.1 Observations and reduction.

Experiments were carried out using Ajisai since it is relatively easy to obtain a large variation in received energy from the large target. The variation from single photon to multiple photon levels was achieved during the experimental passes by altering the divergence of the laser beam and hence the energy density at the satellite. The observations were filtered in the standard way, by using them to solve for corrections to the predicted orbit. However, it was found that this process did not remove all trends from the range residuals, indicating the presence of systematic range biases which varied during the passes. We found that it was necessary to divide each pass into a number (6) of segments, and use the processing software to filter the observations in each segment separately. The resulting scatter plot for one of the experimental passes is shown in Figure 4. The residuals from each of the six segments are shown in histogram form in Figure 5, along with the standard deviations of the fitted Gaussian distributions.

We calculate the average percentage return rates at intervals of 30 seconds throughout the passes by counting the numbers of satellite returns and the numbers of pre-return noise detections. Given that the laser fires 10 shots per second, the true percentage return rate in each 30-second interval is then

(number of true range measurements*100)/(30*10 - number of noise events)

On the assumption that the quantum efficiency of the SPAD is 20%, we calculate from these corrected return rates the average numbers of photons in each return. However we found that in several of the 30-second intervals the calculated return rate was nearly 100%. At such return levels we cannot reliably estimate the mean number of returning photons, which may be far in excess of the 16 estimated for a near 100% rate. Where possible, we have used these 30-second mean values to estimate the mean numbers of photons contributing to the observations in our 6 segments, and these averages are shown in Figure 5. For those 2

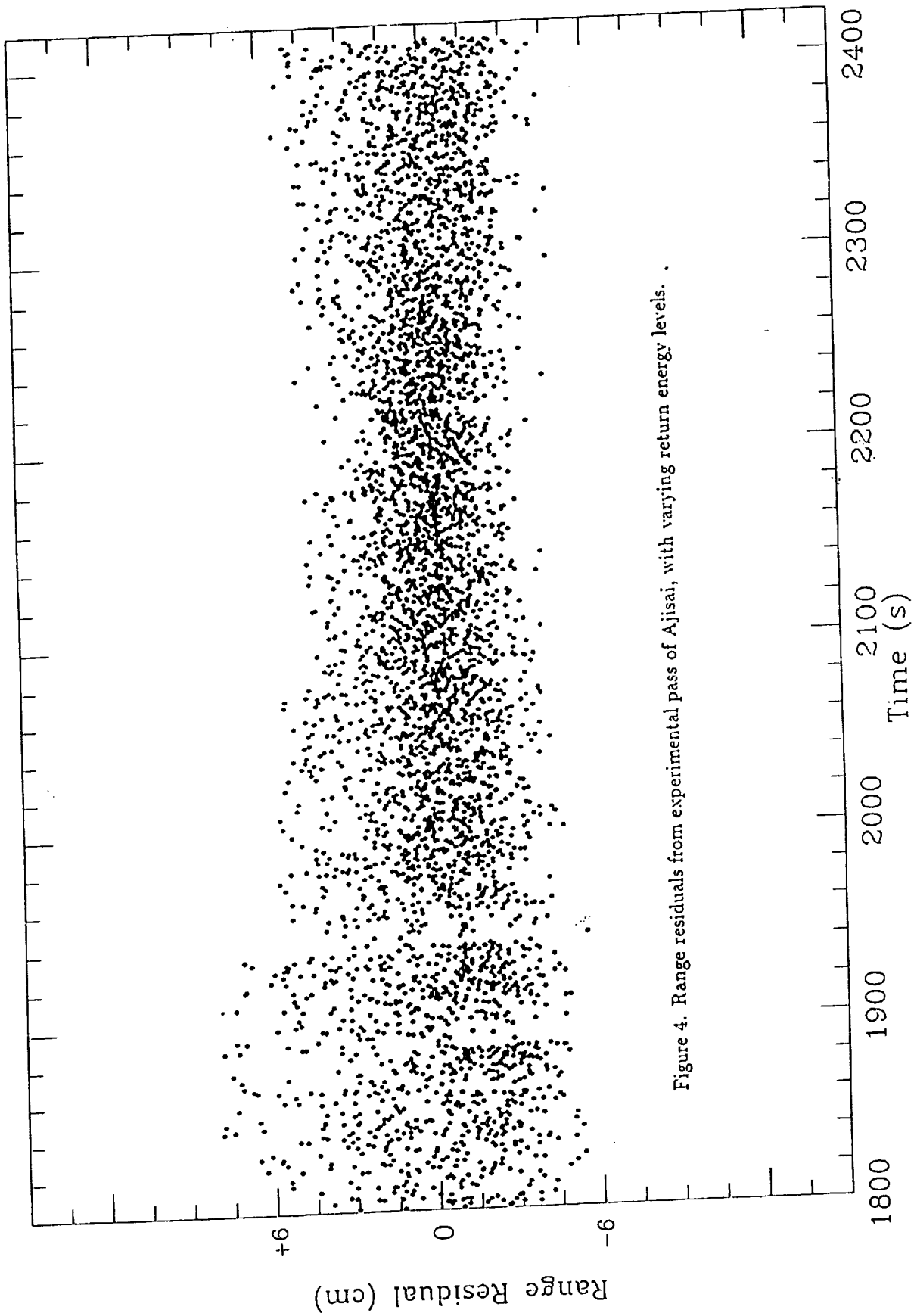

Figure 4. Range residuals from experimental pass of Ajisai, with varying return energy levels. .

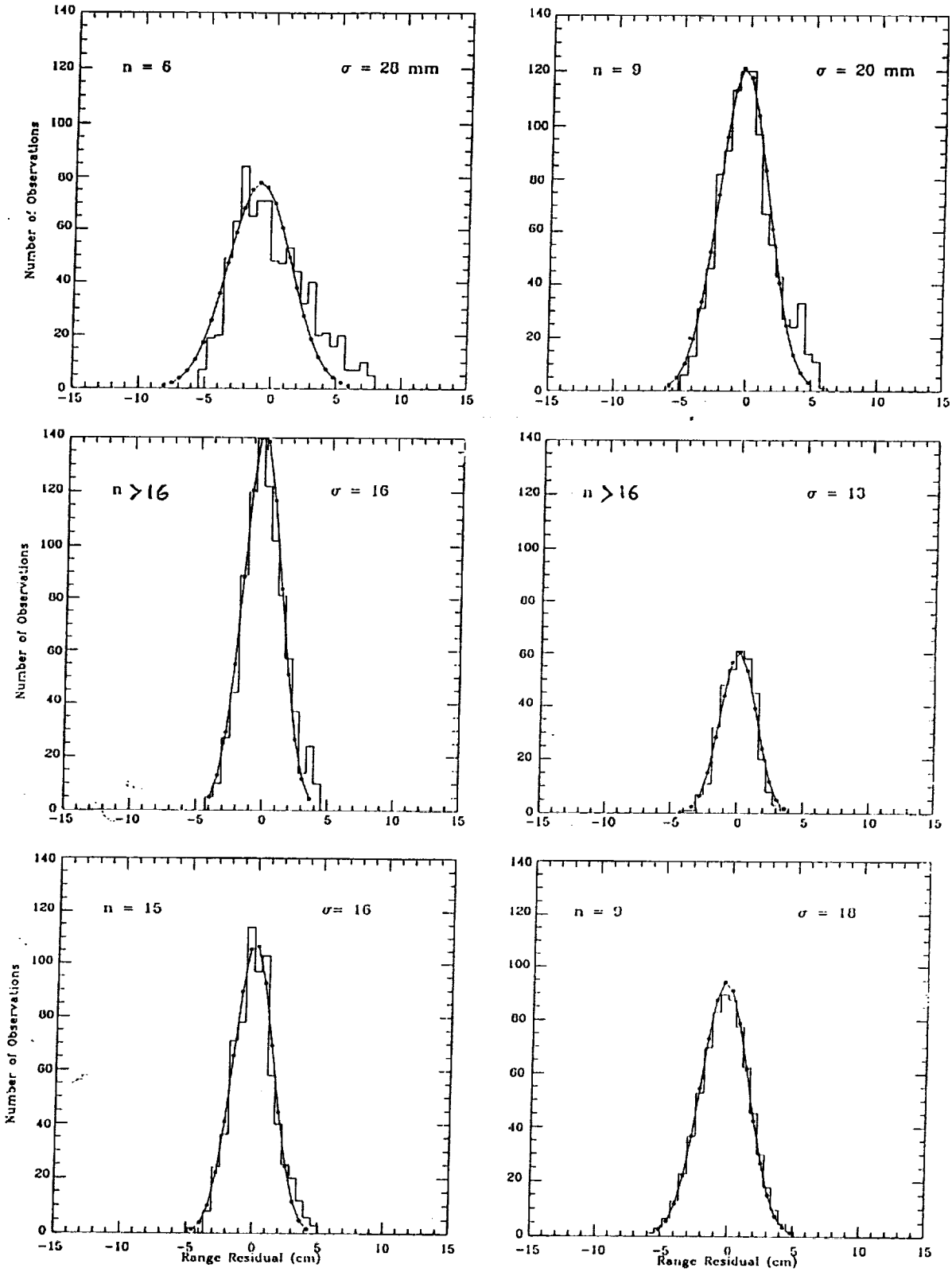

Figure 5. Distribution of range residuals from Ajisai pass as a function of average numbers n of returning photons.

segments where the average return rates were near 100%, we have asigned the numbers of photons as >16, but remark that the true numbers could be several times as large.

4.2 Model and Discussion.

There is a clear variation of histogram shape and single-shot precision with change of signal strength. At low return rates equivalent to single photon returns, the distribution of residuals is similar to the 'standard' Ajisai distribution (Figure 1). For the high return rates little of the satellite signature remains in the distributions, and the histograms qualitatively and quantitatively resemble those from Starlette or ERS-1 (Figure 1).

These results cannot be used to detect a systematic variation of satellite mean reflection distance during the passes, because the method of reducing the observations absorbs any such corrections. However we can use models to predict both the increase of precision and this change of mean reflection distance as a function of numbers of photons in each return. We model the time-distribution of the returning photons, from which we may sample a variable number, by convolution of the Ajisai spread distributions with a Gaussian distribution of FWHM 50 ps, to represent the laser. To model the effect of n photons reaching the detector, we use a random number generator to pick one 'photon' from our time-distribution of photons, then record its time-location within the distribution, and repeat the process n times. We then sort this sequence of n relative event times into chronological order of arrival at the detector. We model the 20% efficiency of the detector by stepping through the n events in time order, at each step generating an integer random number in the range 1-5. If the random number is 1, the event is accepted (detected). If the random number is not 1, the next event is 'tested'. In this way we generate a large number of event times each resulting from the selection of a single photon from a series of returns containing an average of n photons. The mean and standard deviation of these event times are computed and converted to range in cm. The standard deviation values are added quadratically to the estimated system jitter (0.8 cm) to fully model the observations. The results of simulations of range precision and biases from Ajisai for values of n between 1 and 50 are shown in Figures 6a and 6b, where the results have been joined by continuous lines. The 30-second average observed values of precision, where they can be reliably estimated (see section 4.1) from our experimental Ajisai passes, are shown as dots on the graph and agree well with those predicted. The predicted range bias curve in Figure 6b expresses the expected change of mean reflection distance from the satellite centre of mass as a result of increasing the number of photons reaching the detector in each laser return. Most of the bias, which contains a contribution from the finite pulse length of the laser (FWHM 50ps), is seen to take effect between signal strengths at the single photon level up to an average of about 40 photons per return. Little change is predicted with increasing numbers of photons beyond that point.

4.3 Lageos Centre-of-mass correction.

We can use the above techniques to estimate the magnitude of a systematic range-bias for Lageos, in the context of worldwide SLR systems working at different return-signal levels. Figure 6 shows the results of a computation of the range bias as a function of average number of photons reaching the detector, for 2 modelled laser pulse-lengths. The magnitude of the change of the effective reflection distance from the satellite centre of mass is about 1.3 cm for a variation of return level from single-photons to the 40 photon level. This result

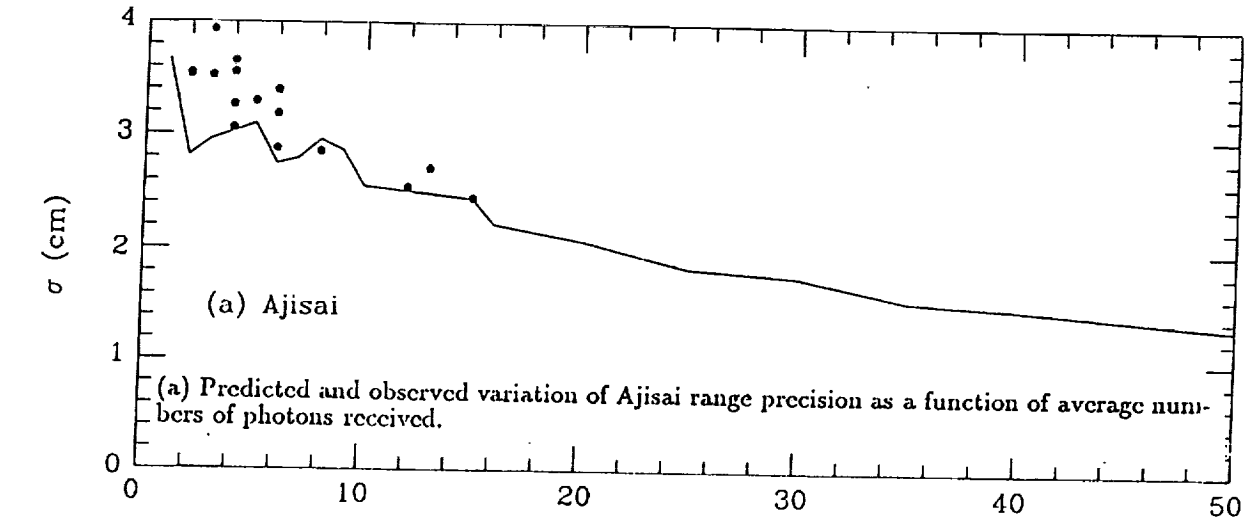

(a) Predicted and observed variation of Ajisai range precision as a function of average numbers of photons received.

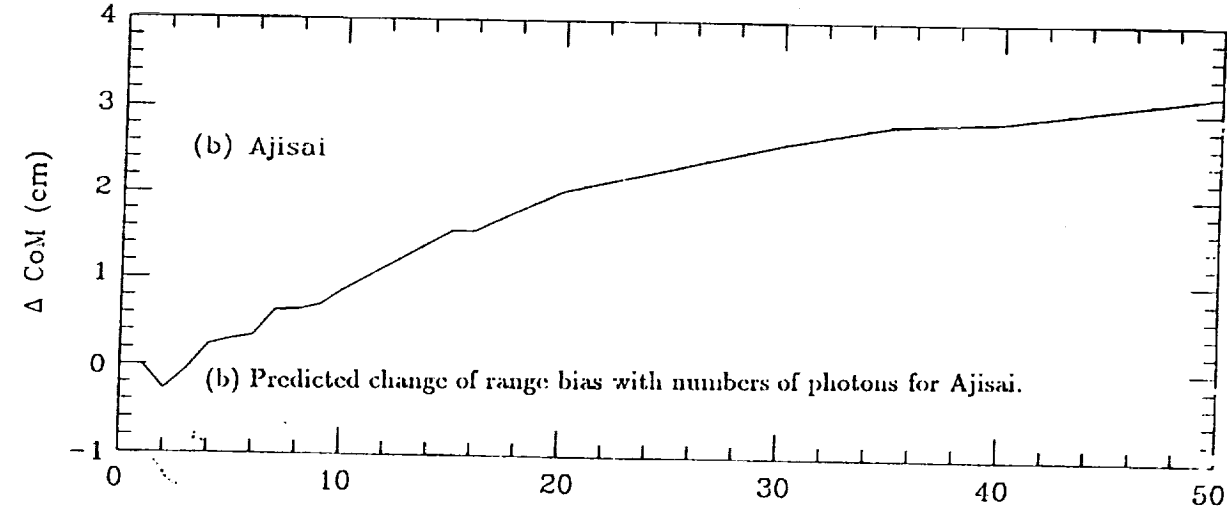

(b) Predicted change of range bias with numbers of photons for Ajisai.

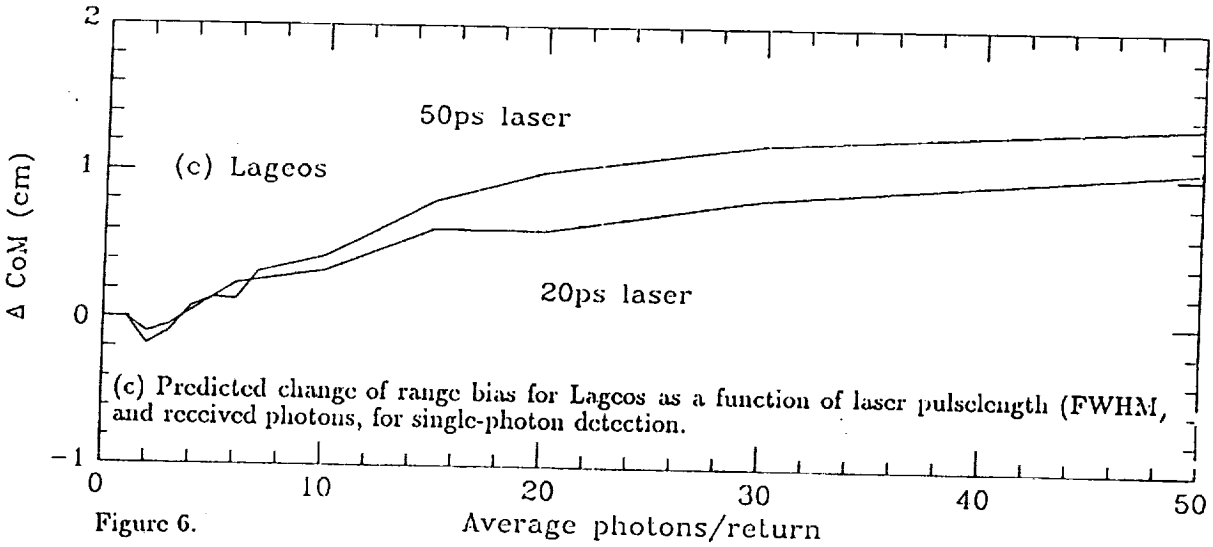

(c) Predicted change of range bias for Lageos as a function of laser pulselength (FWHM, and received photons, for single-photon detection.

Figure 6.

implies that an SLR system receiving and detecting single photons, and using a laser with a pulsewidth (FWHM) of 50 ps, is on average effectively observing a distance 1.3 cm closer to the satellite centre of mass than a single-photon detection system receiving more than about 40 photons per shot. Removing from this figure the effect of the length (FWHM) of the laser pulse, the satellite-induced range bias amounts to about 0.6 cm. The recommended centre-of-mass correction for Lageos is 25.1 cm for leading-edge, half-maximum detection of a large return pulse, and 24.9 for peak detection (Fitzmaurice *et al*, 1977). We assume that the electronic detection of the peak of a large return pulse is equivalent, in terms of distance from cenre of mass, to the formation of the mean of a set of range residuals arising from the detection of single photons. For the Herstmonceux system working at the level of single photon returns, the appropriate centre-of-mass correction should therefore be the same as for the large-pulse, peak-detection systems, *ie* 24.9 cm. However, for single-photon systems departing from the single photon regime, the implications of this investigation are that the centre of mass correction should be *increased* from the 24.9 cm by an amount as given in Figure 6, depending upon the laser pulse-length and the number of photons reaching the detector.

5. Conclusion

Using observations from the UK single-photon SLR system, we have demonstrated that the observational scatter contains a satellite-dependent signature, and that this signature varies as expected with the number of photons reaching the detector. The implications of this variation upon the corrections required to relate range observations to the centres-of-mass of the satellites is modelled and discussed. The magnitude of the effect is system-dependent since it depends both on the number of photons reaching the detector, and hence on laser energy level and local atmospheric conditions, and upon the laser pulse length. A graph is presented giving a calculated, energy and pulse-length dependent, center of mass correction for Lageos range data obtained using single-photon detection, which varies by 1.3 cm over the range of the parameters considered.

6. Acknowledgements

All of the observations reported here were carried out by the SLR team at Herstmonceux, East Sussex, UK, under the direction of the station manager Dr. Roger Wood. The team's interest in carrying out the non-standard observations is appreciated. I thank Dr. Andrew Sinclair, Head of the RGO Space Geodesy Group, for his comments throughout the work on this project.

7. References

Fitzmaurice, M.W., P.O. Minott, J.B. Abshire and H.E. Rowe. 1977. *Nasa Technical Paper 1062.*

Gardner, C.S. 1976. Effects of random path fluctuations on the accuracy of laser ranging systems. *App. Optics, Vol 15, No. 10.*

Prochazka, I., K. Hamal and B. Sopko, 1990. Photodiode Based Detector Package for Centimeter Satellite Ranging, *Proc. 7th Int. Workshop on Laser Ranging Instrumentation, Matera, Italy, 1989.*

Sasaki, M and H. Hashimoto. 1987. Launch and Observational Programme of the Experimental Geodetic Satellite of Japan. *IEEE Trans. on Geoscience and Remote Sensing, Vol GE-25, No. 5.*

N94-15558

Work at Graz on Satellite Signatures

Georg KIRCHNER, Franz KOIDL

SLR Graz / Institute for Space Research
Austrian Academy of Sciences
Observatory Lustbühel, Lustbühelstr. 46
A-8042 GRAZ, AUSTRIA

Tel.: +43-316-472231; Fax: +43-316-462678
E-Mail: kirchner@flubiw01.tu-graz.ac.at

Abstract

The size and shape of the satellites retroreflector arrays have a major impact on the distribution and scatter of the return signal; this can be seen clearly when reaching sub-cm ranging accuracies and when using Single-Photon Detectors with single- or multi-photon returns; for other receiver systems (using MCP's) it should be checked also. As a consequence, the necessary center-of-mass correction for some satellites will different, depending on the receiver systems.

While this effect is not yet visible on small satellites or small retro-reflector arrays (like STARLETTE, ERS1), it can be in the order of centimeters on AJISAI or ETALON.

1.0 Introduction

The SLR station Graz uses, since some years, Single Photon Avalanche Diodes (SPAD) to detect return signals from satellites; these diodes can detect single photons - which is used for ranging to ETALON, or, in worse atmospheric conditions, also for lower satellites -, but usually we use multiphoton returns to get maximum return rates; this results in better accuracies when using Normal-Point-Methods, and helps to avoid part of the

satellite signatures in the return signal distribution, as described later.

2.0 Ranging tests to the calibration target

Standard calibration to our target (distance about 400 m) gives an RMS of 6 to 7 mm for the routine SLR setup (with HP5370A counter, SPAD at 10 V above break, cooled to -27°C; 2.5σ limits); an example is shown in fig. 1, upper histogram; the distribution shows nice symmetry, with an RMS of 5.8 mm at 2.5σ ; there is no significant change of the mean value when using different sigma criteria, also indicating a proper distribution.

To check influences of the ranging system itself on the distribution of the return signals, different tests with various misadjustments of the involved devices were made; a worst-case example is shown in fig. 1, lower histogram: A similar calibration as before, but with misaligned SPAD, lower voltage above break, no cooling, and non-optimum start puls detection; this results in a non-symmetric distribution, higher RMS, and measurable shift of the mean value for varying sigma criteria.

After verifying the maximum contribution of the system itself, the distribution of returns from different satellites were analyzed.

3. ERS1 and STARLETTE

Due to their small size of the retroreflector arrays, there is no significant satellite signature visible in ERS1 and STARLETTE data; the average RMS is between 8 and 9 mm, close to the values obtained from the calibration target.

The distribution of the data (fig. 2, upper histogram) is more or less symmetric, with small irregularities due to lower number of returns; the 3 mm bin width for all these histograms was chosen in coincidence with the 20 ps resolution of the HP 5370A counter.

4.0 AJISAI

As a contrast to the previous satellites, AJISAI shows quite significant signatures; these are very dependant of the return signal strength (fig. 3).

With strong (multiphoton) return signals, AJISAI shows low RMS (11.8 mm, upper histogram), and only slightly non-symmetric distribution; when reducing the return signal level to mostly single photon-electrons (by switching off the last laser amplifier, and opening divergence; the return signal level is checked in real time by watching the return signal rate and/or the number of semi-train returns on a graphic screen), the RMS increases to 22 mm (lower histogram), while the distribution now follows the shape of the satellite.

Both histograms in fig. 3 are shown with editing criteria of 2.5 σ, which is used for our routine ranging procedures; using other σ values (4 σ, 3 σ, 2 σ), the mean value of the histogram will move - in the worst cases - between 1 and almost 2 cm.

5.0 LAGEOS

As expected from size and shape of LAGEOS, the satellite signature is much less visible than with AJISAI, but is still present (fig. 2); it is the main contribution to the increase of the RMS, from 6 to 7 mm from the target, to 11 to 14 mm from the satellite (again, this is valid for our single-photon detection system, using single photon and/or multi-photon return signals!!), with lower signal levels resulting in higher RMS.

When using different editing criteria again, the non-symmetric distribution causes a shift of the mean value of about 1 to 2 mm, only in extreme cases up to 4 mm.

6.0 ETALON

To complete the satellite's list, we show also the signature coming from ETALON ranging data, this time using a different way

of demonstrating the non-symmetric distribution. While fig. 4 shows the residuals of an ETALON-2 pass (demonstrating also the advantage of using the semitrain!), in fig. 5 the residuals are plotted after "folding", polynomial fitting and 2.5σ-editing. Due to the low return signal level from these satellites (most of the returns are single photons: We are ranging with 5 to 10 mJ Semitrain - this is about 2 or 3 mJ for the first pulse! - and 50 cm receiver to the ETALONS, still getting return rates of up to 1000 returns per hour), we see the full satellite's size and shape in the data, with an RMS of 3.5 to 4 cm

7.0 Conclusion

To keep systematic errors due to the influence of the satellite's shape as low as possible, we

- keep calibration and satellite return signals in the same level
- use the same editing criteria (2.5 σ) for calibration and for satellite data;
- try to minimize any contributions of the system itself to non-symmetric distributions.

As far as we know, in all analyzing calculations the satellites are treated as a "flat" reflecting surface, with a fixed center-of-mass correction, which was determined before launch using the detectors, techniques and accuracies available at that time. However, with the improvements in accuracy, we can see now the shape of the satellites in our data, which in turn can influence the values of the center-of-mass corrections; so it seems necessary to determine the center-of-mass correction with respect to different receiver systems, and using different values for the analysis.

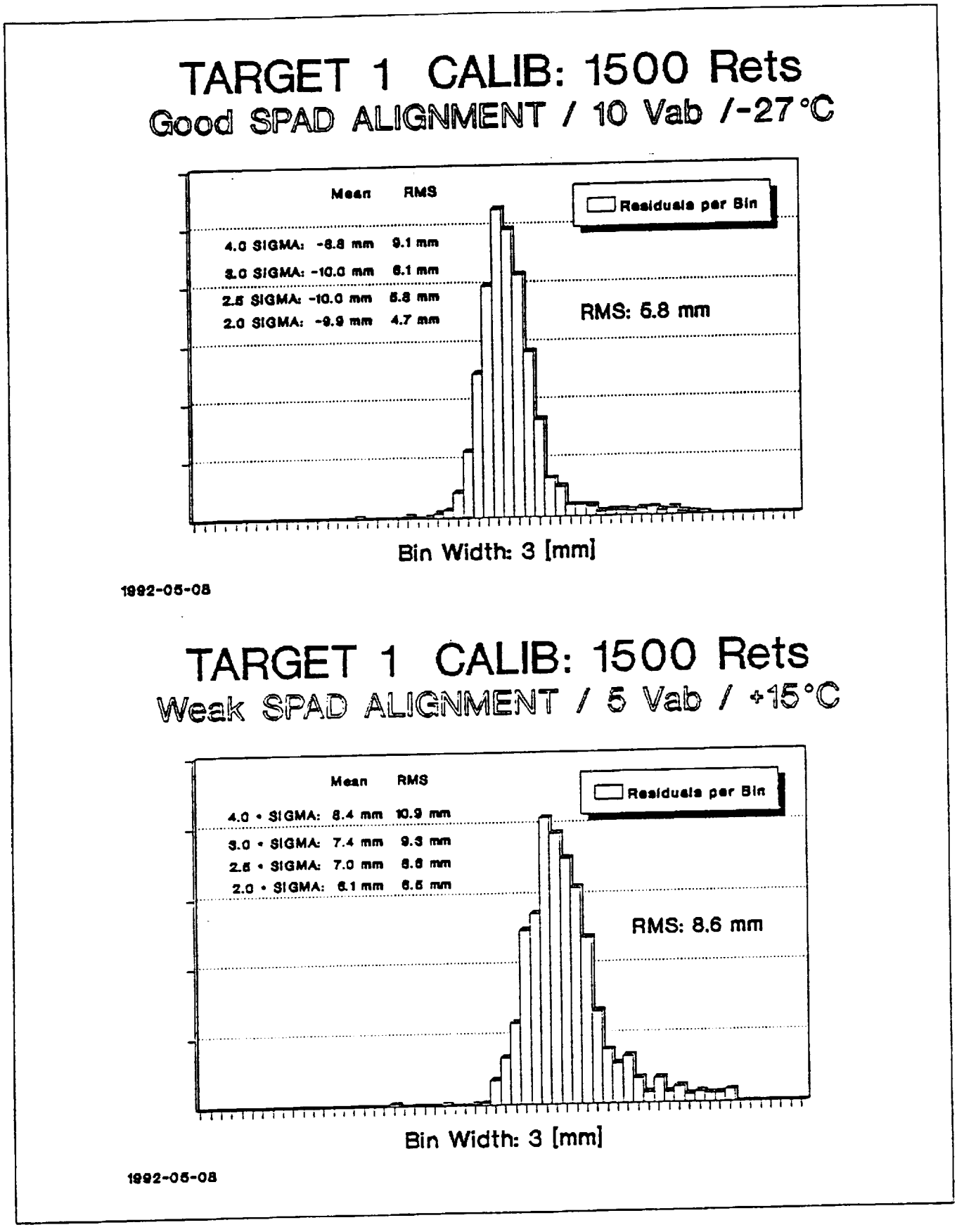

Figure 1: Histograms of calibration ranging to the target

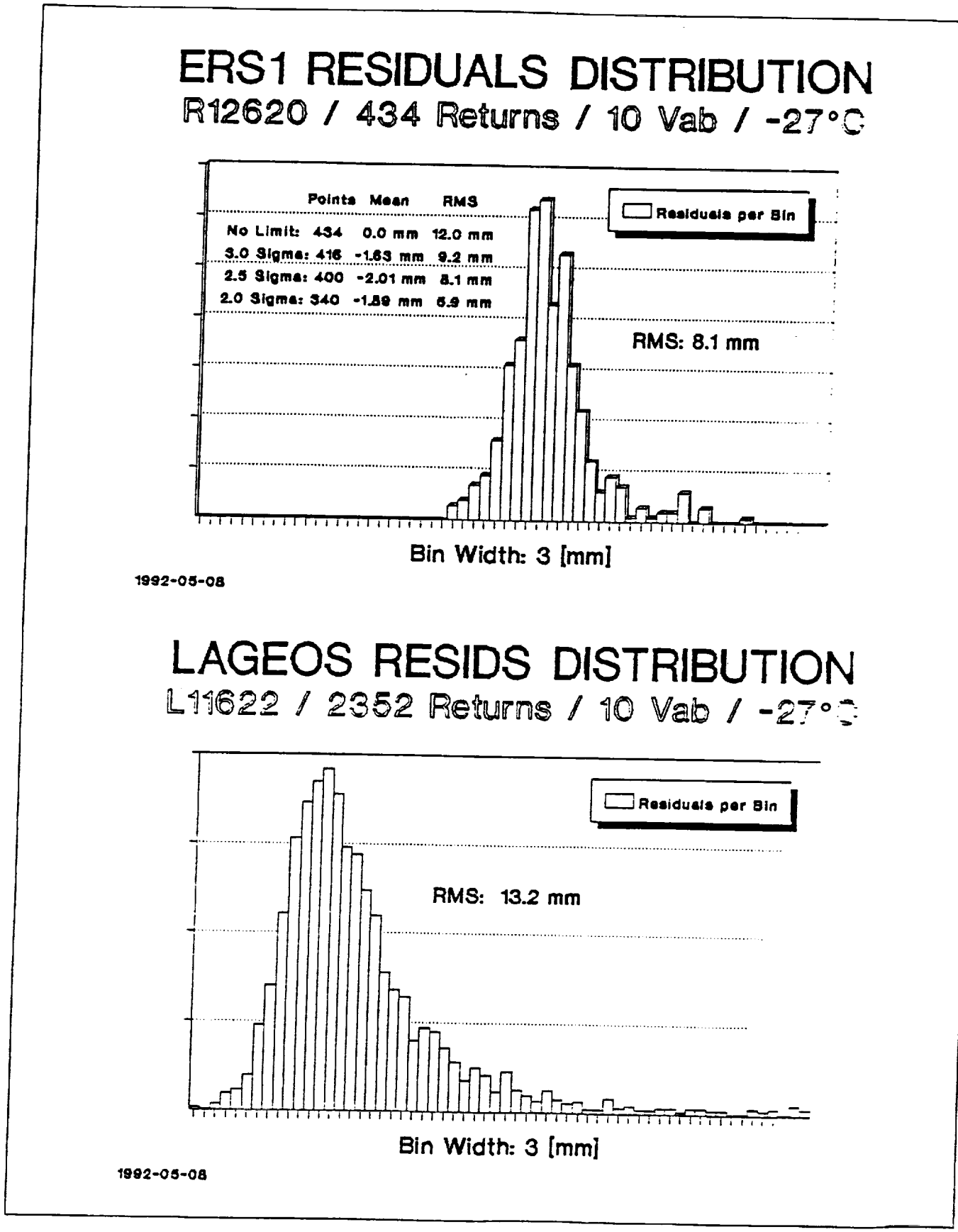

Figure 2: Histograms of ERS1 and LAGEOS returns

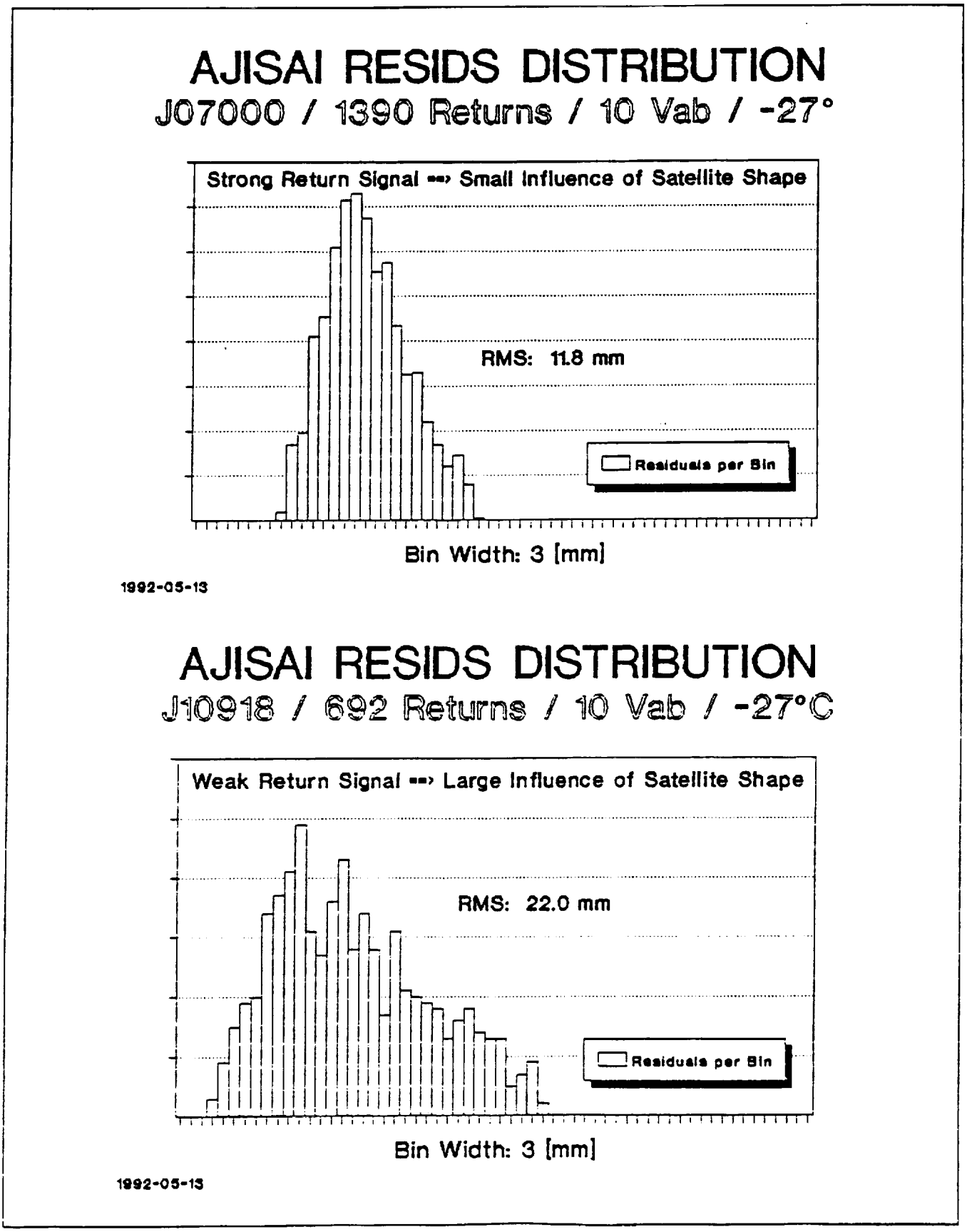

Figure 3: Histograms of AJISAI returns

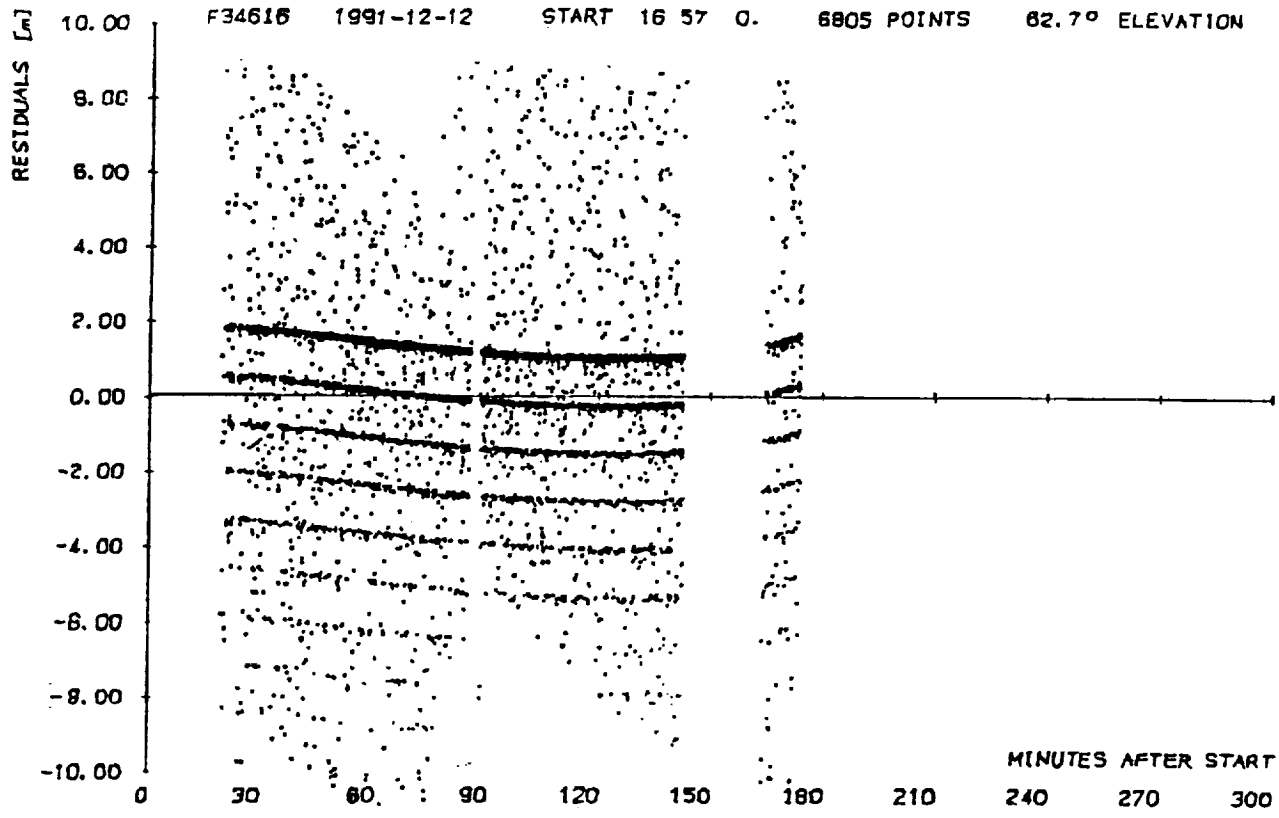

Figure 4: Residuals of ETALON-2, showing semitrain returns

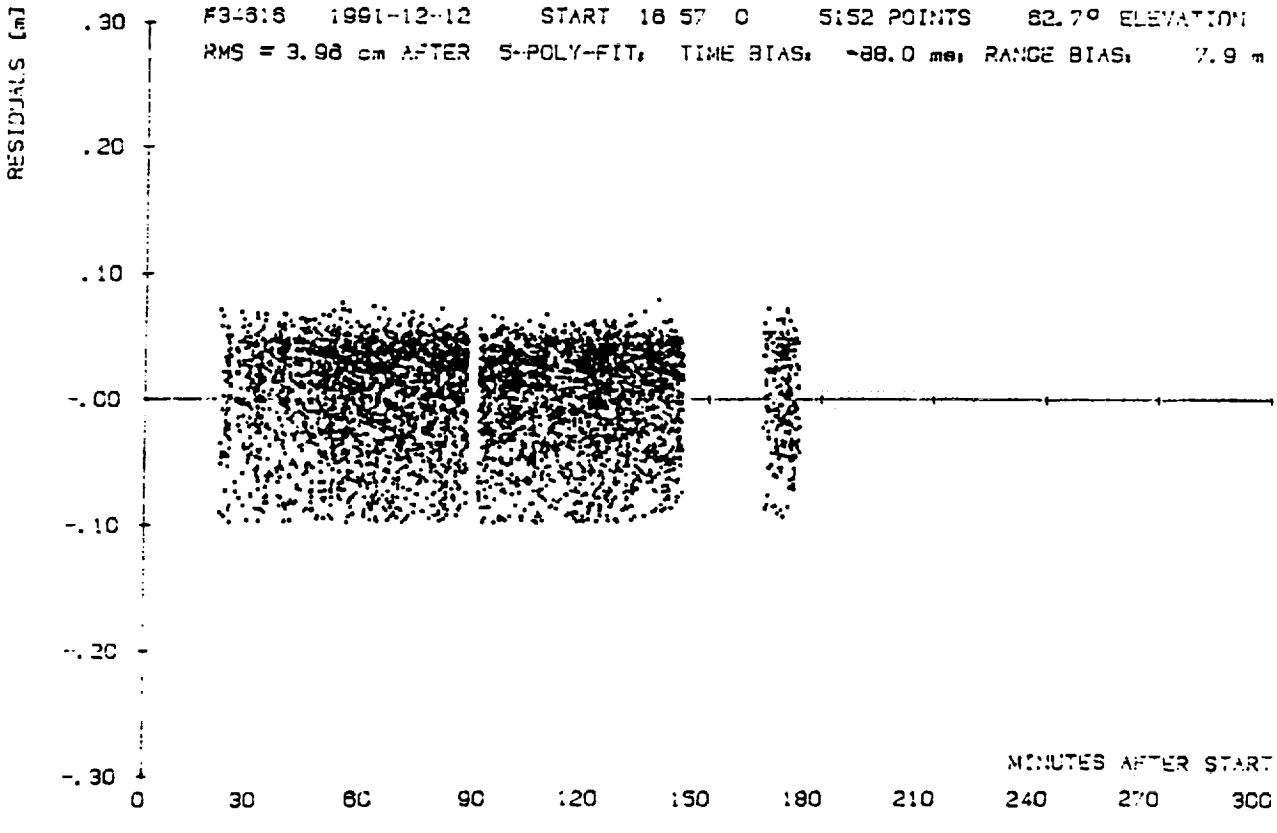

Figure 5: Same ETALON-2, with non-symmetric distribution

N94-15559

THE PRECISION OF TODAY'S SATELLITE LASER RANGING SYSTEMS

P.J.Dunn and M.H.Torrence, Hughes STX Corp., Lanham,MD
V.Hussen, Bendix Field Engineering Corporation, Greenbelt,MD
M.Pearlman, Smithsonian Astrophysical Observatory, Cambridge,Mass

Introduction

Recent improvements in the accuracy of modern SLR systems are strengthened by the new capability of many instruments to track an increasing number of geodetic satellite targets without significant scheduling conflict. This will allow the refinement of some geophysical parameters, such as solid Earth tidal effects and GM, and the improved temporal resolution of others, such as Earth orientation and station position. Better time resolution for the locations of fixed observatories will allow us to monitor more subtle motions at the stations, and transportable systems will be able to provide indicators of long term trends with shorter occupations. If we are to take advantage of these improvements, care must be taken to preserve the essential accuracy of an increasing volume of range observations at each stage of the data reduction process.

The Range Measurement

The SLR measurement is computed as one half of the product of an adopted value of the speed of light and the observed interval between the transmit time of the pulse and the time of a detected return. The essential simplicity of this process is tempered by the need for careful calibration for system delay and atmospheric refraction, as well as for an accurate survey of mount eccentricity and other important local coordinates to match the millimeter accuracy of the best current systems. The influence of satellite signature and detector time-walk must also be considered at this high accuracy level, and we consider here the particular need to preserve any details of these effects which may be lost in the current normal point compression process.

Normal Point Generation

The loss of detail at each stage of the process to reduce engineering data to normal points is illustrated in Table 1, which shows the information content of each of the parameters measured by most instruments for a typical satellite pass or pass sequence. Information on receive energy level is not necessary if all time-walk characteristics of the detector system have been eliminated or corrected before data compression. Neither will the absence of calibration details matter if the distribution of returns is identical to that from the satellite and the same algorithm is applied to reduce each observation. The accuracy of the satellite observations will be preserved as long as the return distribution is normal (or Gaussian) about the mean range.

Shape Factors

Two measures of the deviation of a distribution from normal are illustrated in Figure 1. Any skewness in the pattern of range residuals about the mean would bias normal points if we assume that the peak of the distribution is a better measure of the range. Skewness is computed from the third moment of the residual distribution, just as the standard deviation is based on the second moment: it is positive for a distribution with a tail towards long ranges, and negative (a rare

occurrence) when the noise is short. Another shape factor can be simply obtained as a combination of third and fourth moments: kurtosis gives an indication of flatness (low values) or peakiness (high values). A residual histogram with low kurtosis values can be produced by using a lower value of the sigma multiplier than three for data editing (clipping); high kurtosis values are obtained when a larger sigma multiplier than three is employed, and the return signal appears as a spike in the background noise.

Interpretative Aids

The utility of these shape factors can be demonstrated with examples from several different systems. To illustrate the mechanism used to build the basic contour picture which we have adopted for data quality assurance we refer to Figure 2, which is a three-dimensional accumulation of a number of pass histograms for LAGEOS ranges taken at the Grasse Observatory during a three month interval. The vertical scale shows the percentage of range measurements which lie within ten millimeter bins distributed about the mean value. An imaginative reader will observe a progression from a nearly symmetrical distribution in December 1990 to a significantly skewed pattern in February 1991: the front profile on 91-02-27 demonstrates the characteristic of long noise. The coarse grain caused by the centimeter bin width is softened in the contour of the same data which is shown in Figure 3. The grey band of the contour scale shows a shift in the distribution in early January 1991 and the lighter peaks also suggest a change in character at this time: the darker contour levels emphasize the asymmetrical tail towards long ranges in January and February 1991.

Quantifying the residual behavior

Numerical descriptors for the changing residual pattern are shown in the scatter plot to the left of the contour frame. The crosses depict a normalized skew factor which jumps from a low (moderately skewed) to a high value at the same time that a low (flat peak) kurtosis measure returns to a nominal level as shown by the open circles. The change in the pattern was caused by a relaxation of the tight data editing criterion applied to the earlier observations which clipped the distribution and muted the intrinsic asymmetry exposed with more liberal editing. The standard deviation of the full-rate data is recorded with the normal points in the currently adopted compression scheme, so this event would be flagged as an increase in noise level, but the skew and kurtosis shape factors provide improved diagnostics at a relatively low computational cost.

The cause of any data asymmetry can be isolated by inspecting the distribution of the calibration measurements: if the asymmetry is restricted to the satellite returns, the shift in the effective range measurement due to the editing change would amount to over a centimeter and would cause an even larger change in the apparent height of a station position determined from these observations. On the other hand, similar levels of asymmetry in the ground target returns would suggest a source in the detector rather than the satellite, and if the same editing scheme was used for each data type, there would be no bias in the satellite measurements.

Satellite and Calibration Target Data

We have considered the shape of distributions from calibration and satellite targets in an analysis of observations from six GSFC systems collected in early 1992. Figure 4 shows a collage of residual histogram contours from the systems tracking several different satellites: ERS-1(E), Starlette(S), LAGEOS(L), Ajisai(A), ETALON-1(E1), and ETALON-2(E2). This broad representation shows at a glance the higher noise level of the ETALON satellite returns, as well as the tight

precision of data from lower-orbiting satellites like ERS-1, which amounts to about 5 millimeters for MOBLAS-7. The same ten millimeter bin scale is used to describe the characteristics of these instruments as for the data from Grasse in the earlier example.

The patterns for the appropriate calibration passes are given in Figure 5: they show less variation than the satellite data, and allow us to discriminate satellite-dependent variations from detector characteristics. None of the systems depicted here shows a systematic bias of more than a millimeter, but subtle effects in the distribution for an individual system can be detected and quantified by the skew and kurtosis shape factors plotted in the Figures provided for a couple of the instruments. The satellite returns for Moblas-7 show no consistent kurtosis but a hint of the positive skew typical of all systems' observations of the ETALON satellites (at the bottom of the plot); the MOBLAS-7 calibration returns are slightly clipped (low kurtosis). On the other hand, TLRS-4's satellite returns show no significant skew, but indicate a hint of clipping; this instrument's calibration data possesses the rare property of slight negative skewness.

Summary

The effects of these idiosyncrasies in residual pattern for the GSFC systems is well below the accuracy threshold for any currently employed application of the data, but they could be used to characterize subtle changes in system characteristics. We have attempted to demonstrate in the above examples the enhanced ability to monitor data quality for any SLR system with some simple shape factors which can be computed economically in the normal point compression stage. Regular inspection of these parameters can flag changes in data characteristics which affect range accuracy, and also provide reassurance that our most advanced systems do indeed attain the millimeter accuracy of which they are capable.

LEVEL	DATA TYPE	GRANULARITY				
		ROUNDTRIP		RECEIVE ENERGY		MET.
		SAT.	CAL.	SAT.	CAL.	
0	RAW ENGINEERING	POINT	POINT	POINT	POINT	POINT
1a	PROCESSED FULL RATE	POINT	PASS	POINT		POINT
1b	NORMAL POINTS	BIN	PASS			BIN

TABLE 1: The information content of each data type is diluted in each step of the data compression process, although some statistical properties of the original distribution are recorded.

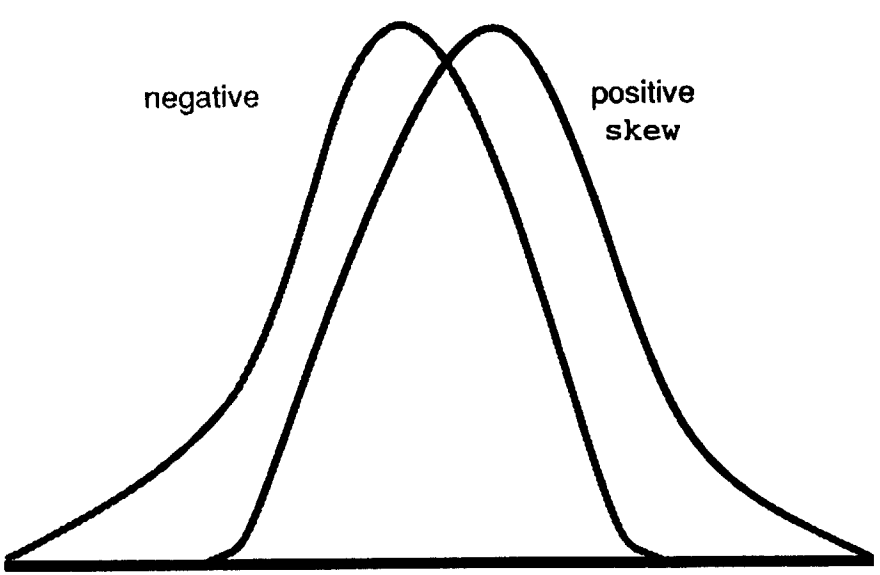

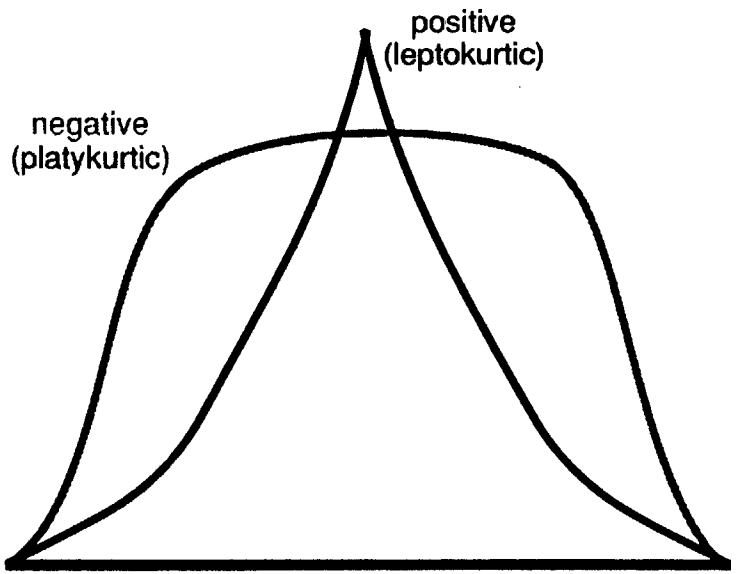

FIGURE 1: Shape factors which characterize the range deviation from normal can be used to supplement the root mean square value which is usually recorded. Slight positive skew is observed in almost all the systems; negative kurtosis(compared to a normal value of 3.0) is seen when a low editing multiplier (<3) "clips" the distribution and positive kurtosis is a symptom of loose editing (>3) which does not reject background noise.

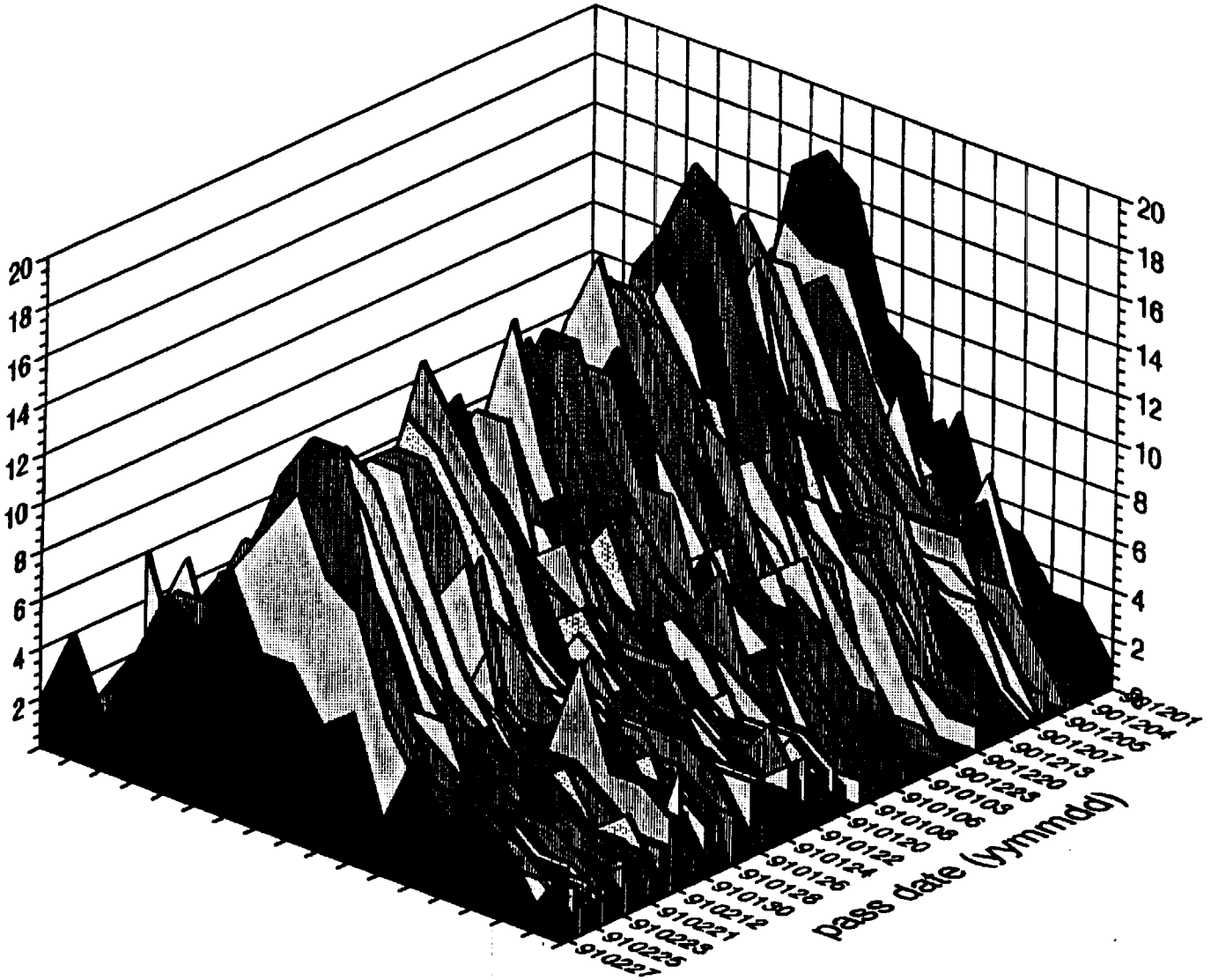

FIGURE 2: The build-up of pass histograms shows a progression towards a skewed distribution with time for LAGEOS data from the Grasse Observatory. The horizontal scale bin width is ten millimeters, and the ordinate gives the percentage of observations within each bin.

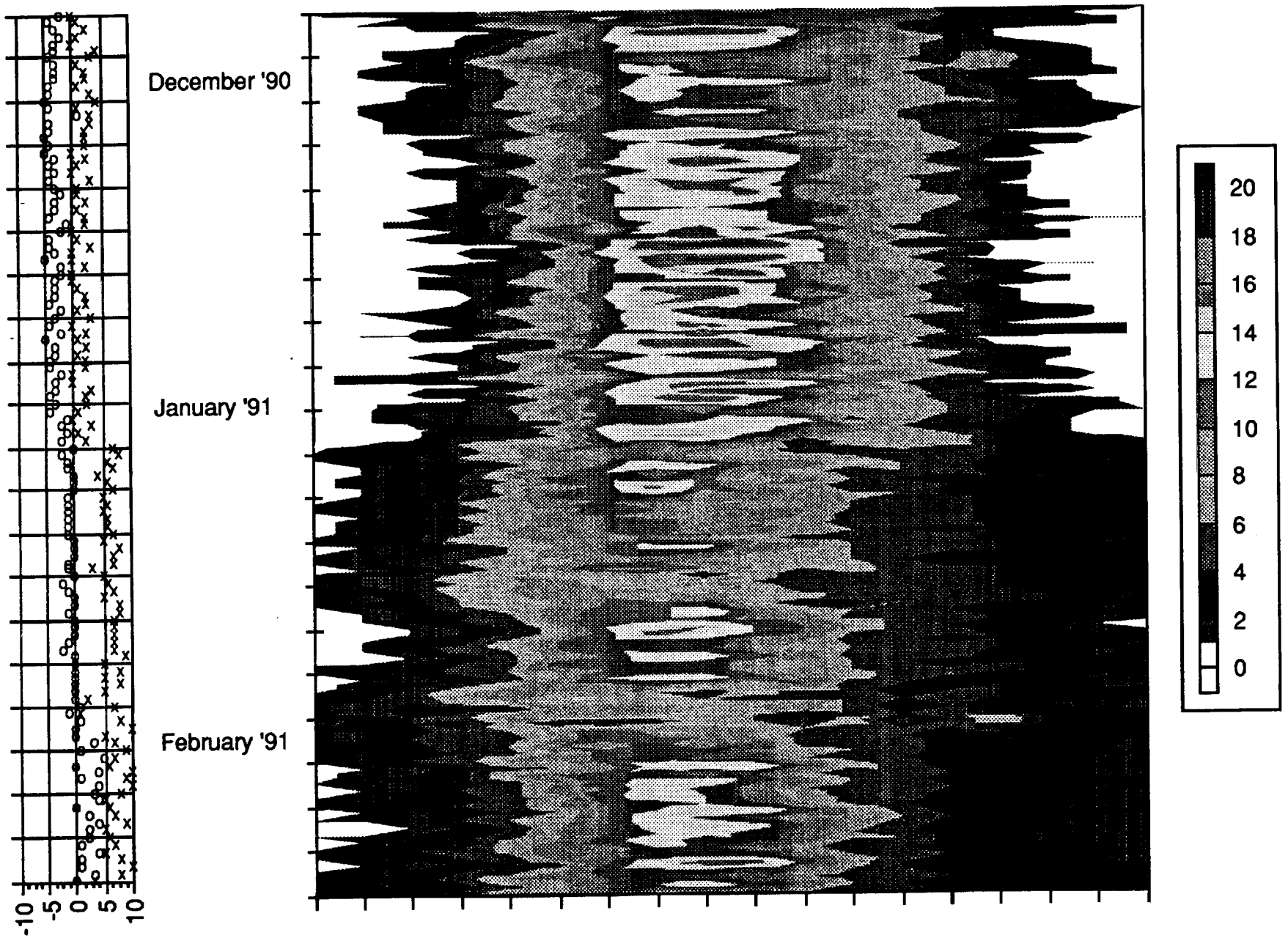

Figure 3. Pass-by-pass 10 mm binned LAGEOS residuals from Grasse.

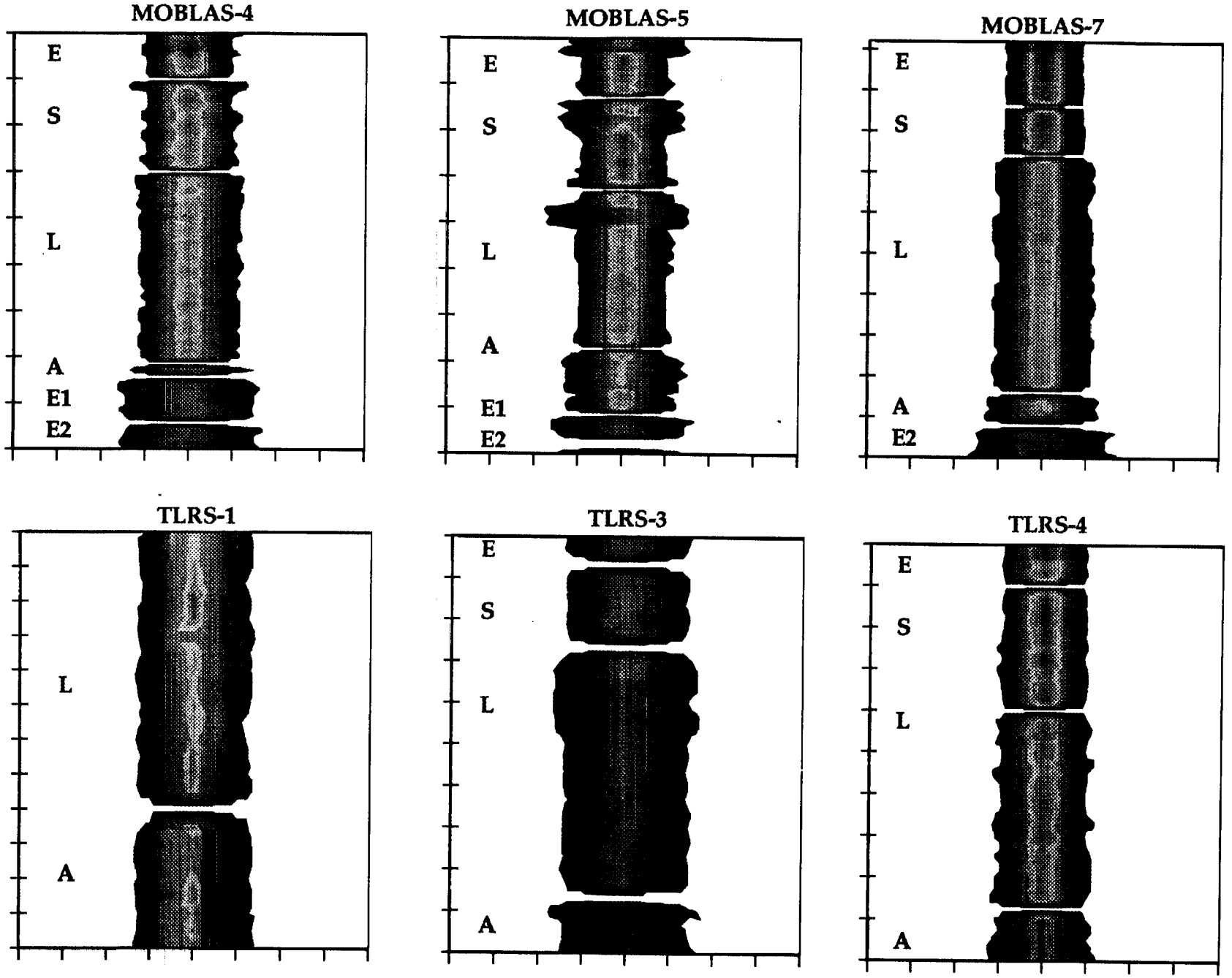

Figure 4. Satellite binned residuals.

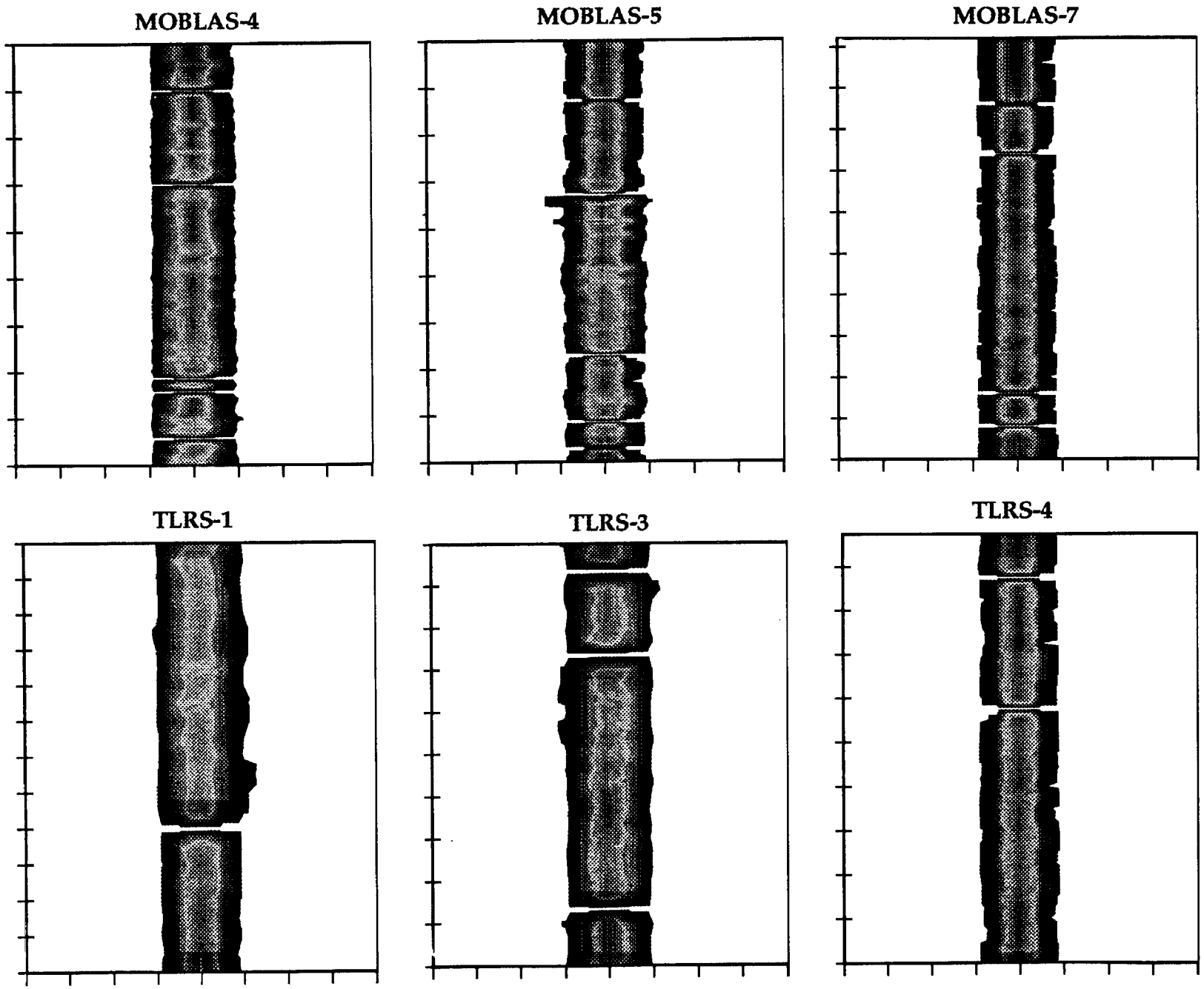

Figure 5. Calibration binned residuals

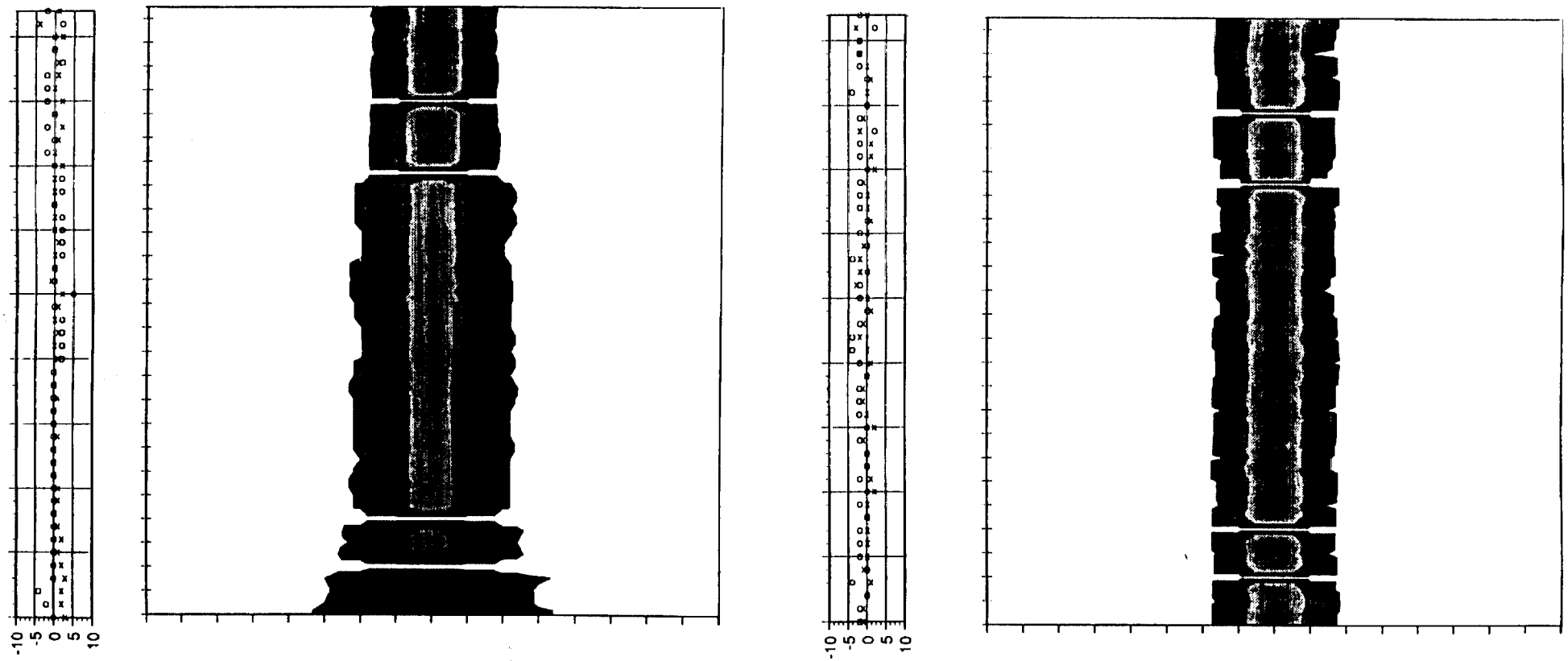

Figure 6a. Satellite and calibration binned residuals from MOBLAS-7

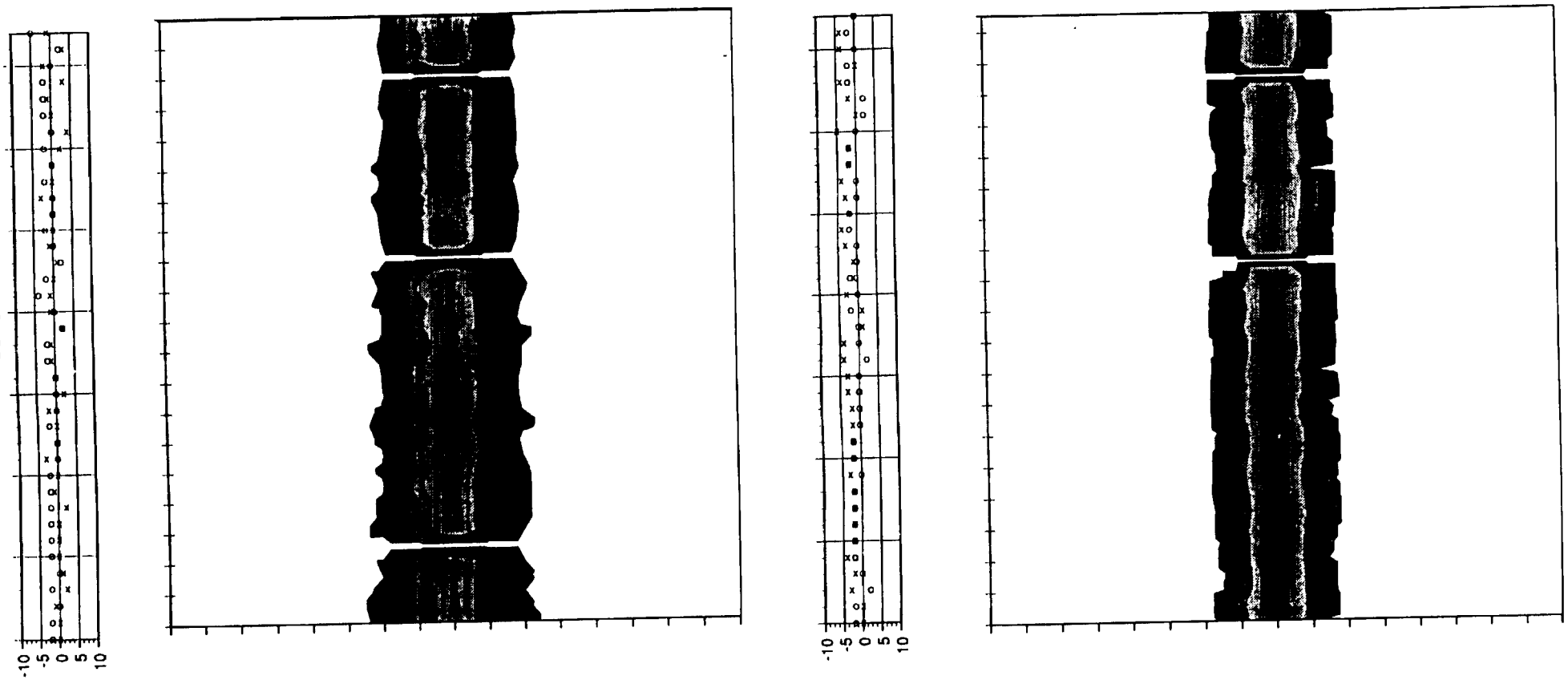

Figure 6b. Satellite and calibration binned residuals from TLRS-4.

N94-15560

SLR Data Screening; location of peak of data distribution

A.T. Sinclair

Royal Greenwich Observatory, Madingley Road, Cambridge CB3 0EZ, England

1. Introduction

At the 5th Laser Ranging Instrumentation Workshop held at Herstmonceux in 1984 consideration was given to the formation of on-site normal points by laser stations, and an algorithm was formulated. The algorithm included a recommendation that an iterated 3.0 × rms rejection criterion should be used to screen the data, and that arithmetic means should be formed within the normal point bins of the retained data. From 1990 September onwards this algoritm and screening criterion have been brought into effect by various laser stations for forming on-site normal points, and small variants of the algorithm are used by most analysis centres for forming normal points from full-rate data, although the data screening criterion they use ranges from about 2.5 to 3.0 × rms. At the CSTG SLR Subcommission a working group was set up in 1991 March to review the recommended screening procedure. The working group consists of A.T. Sinclair (chairman), G.M. Appleby, R.J. Eanes, P.J. Dunn and T.K. Varghese. This paper has been influenced by the discussions of this working group, although the views expressed are primarily those of this author.

The main thrust of this paper is that, particularly for single photon systems, a more important issue than data screening is the determination of the peak of a data distribution, and hence the determination of the bias of the peak from the mean. Several methods of determining the peak are discussed.

2. The effect of skew data

The first stage of forming normal points (described by Appleby in these proceedings) is to fit a trend-function to the raw ranges or to their residuals from a predicted orbit so that all signature from the orbit is removed, and then the distribution of the trend-removed data can be examined. Some level of screening is needed in the iterative process of fitting a trend-function, but this is not critical; 3.0 × rms or perhaps even tighter should be fine, and finally a wider band of trend-removed data, say 5.0 × rms, should be retained for examination of the distribution and then final screening. If these data have a symmetrical distribution about the peak then the criterion used for final screening is not critical, and a 3.0 × rms screening and use of the arithmetic mean should be fine. However if the data have a skew distribution then the arithmetic mean will be biased away from the peak, and the amount of bias will probably be dependent on the level of final screening used.

Analysis of the raw data from numerous stations shows that stations operating at a multi-photon return level per shot tend to have a fairly symmetrical distribution of data, whereas those operating at a single photon return level frequently show a significant skewness in the distribution of the data, usually skewed towards long ranges. As is described in papers by

Appleby and by Kirchner in these proceedings, some satellites (particulary Ajisai) impose their own signature on the laser data and can cause skewness as has been detected by some single-photon systems. However it is probable that some of the skewness is caused by the laser systems themselves, and it is certainly not the intention to explain away features of the system as being due the satellite. However if the skewness is due to the satellite then a means must be found in software of handling it. If it is due to the system then one view is that it is an engineering problem and that the hardware should be adjusted, but another view is that hardware will never be perfectly adjusted, and that one should accept some level of mal-adjustment and calibrate the effect out with software. Also it is possible that some detectors such as avalanche photo-diodes have an inherent skewness which would be very difficult to remove by adjustment of the hardware.

Systems which operate at a multi-photon return level and use pulse-level detection are in effect using hardware to form a mean of the individual photon returns obtained each shot, and so will see little effect from the distribution structure of the individual returns. Systems which operate at multi-photon level and detect the first photon received will primarily see the leading part of the distribution and will see little effect of any skew tail. Hence these system use a hardware method to eliminate any effects of satellite signature, and must ensure that the hardware is set up so as not to cause any biases. The objective of this paper is to devise an equivalent software scheme for systems operating at single photon return levels.

3. Choice of reference point of data distribution

The current recommendation is that the reference point of a data distribution should be the arithmetic mean of the data retained after a 3.0 × rms screening. This may not be ideal for a skew distribution of data.

If a skew data distribution is entirely caused by the laser ranging system, and if the ranges to the terrestrial calibration target have the same skew distribution as the satellite ranges, then it probably does not matter what screening criterion is used, provided the same is used for both calibration and satellite ranging, and it will probably be satisfactory to take the arithmetic mean of the data, even though this does not give the peak of a skew data distribution. However if the satellite is adding a significant contribution to the distribution, or if for some other reason the distributions of calibration and satellite data are different, then it is probably best that some means of processing the data should be devised such that the peak can be located. This is because, in the complicated convolution of the signatures of the system and the satellite, the range represented by the peak corresponds to the distance travelled by a photon from the peak of the laser pulse to the peak reflection point of the satellite (and so the centre of mass correction for the satellite should be that corresponding to peak reflection as determined in pre-launch testing).

Note that for a satellite pass it is not the peak of the trend-removed data for the whole pass that is required, but the peak of the distribution of the data within each normal point bin. This is a problem as there may not be sufficient points within a bin to give a reasonable indication of the distribution. The solution we recommend is that both the peak and arithmetic mean of the whole pass should be determined, and the difference, or bias, of the mean from the peak should thus be determined for the whole pass. Then within each normal point bin

just the arithmetic mean should be determined, but it should be corrected by applying to it the bias of the whole pass.

4. Methods of determining the peak of the data distribution

The usual method to determine the distribution of data is to plot a histogram, but this by itself does not give a good indication of the precise location of the peak. There is some arbitrariness introduced by the choice of bin width, and this is likely to be much coarser than the resolution required for the peak. An improvement can be made by fitting a curve such as a Gaussian profile to the histogram, but this total process is rather complicated, and as a Gaussian profile is symmetrical it will to some extent be influenced by a skew data set and be pulled away from the peak. In this paper we propose and examine three simpler techniques, and compare their performance on a variety of passes tracked by RGO Herstmonceux.

4.1 Data smoothing

After fitting and removing of a trend function, a plot of the data against time should be just a scatter plot about the mean, exhibiting no trend, but possibly not uniformly distributed about the mean. In order to examine this distribution we no longer consider the data as a time series, but just as points as lying along an x-axis, and our requirement is to plot in the y-direction some function describing the distribution of the points. The usual procedure is to plot a histogram, but we consider an alternative, in which each plotted residual is regarded as the most probable location of the measurement, and so we spread (or smooth) the effect of the residual each side of it using a Gaussian probability distribution. The result is that at any given location on the x-axis there will be contributions from all of the residuals, which can be summed and plotted on the y-axis. The peak of this plotted curve will give the most probable mean value of all of the residuals. The mathematical description of the method is very simple. Let $x_i, (i = 1, n)$ be the residuals of the range values from the trend function. Then for a range of values of x at, say, 10 ps intervals, evaluate and plot the quantity y, given by:

$$y = k \sum_{i=1}^{n} \exp[-\frac{1}{2}(x - x_i)^2/\sigma^2]$$

where σ is the somewhat arbitrary standard deviation of the smoothing function, although it would be reasonable to choose a value close to the single shot precision of the system. We regard the scale of y as arbitrary, and k is an arbitrary factor chosen to give some convenient maximum value of y.

Figure 1 shows a series of plots of this distribution function for a pass of Ajisai for a range of values of σ, with the conventional histogram plotted also. Apart from very small values of σ the peak is well-defined, and can be determined precisely. These plots are centred on the arithmetic mean of the distribution, so it is seen that the peak differs from the mean by about 2 cm, showing the large effect of the skewness (which is primarily caused by Ajisai - see paper by Appleby in this proceedings). A problem with the method is that the location of the peak depends on σ. As σ is increased the skewness has an increasing effect on the location of the peak, and in the plots the peak moves to the right by 2.3 mm as σ varies from 40 to 80 ps. A further problem is that for very sparse passes, possibly affected by a

significant amount of noise, the method fails to give a single main peak, or requires a large value of σ in order to do so.

4.2 Tight rejection criterion

The arithmetic mean of a set of data will be biased away from the peak due to any skewness of the data, but the amount of bias will be reduced if a tighter rejection level is used in forming the mean. We look at the effect of using various rejection levels, expressed as multiples of the root mean square difference from the mean (rms). However the rms of the retained data varies and usually gets smaller as the rejection limit is reduced, so for clarity we first determine the mean and rms using a 3.0 × rms iterated rejection level. Then subsequent rejection levels are expressed as multiples of this fixed rms. It also aids convergence with a tight rejection level if the rejection level itself does not vary as the iterations proceed. The table below gives the results of using various rejection levels on the Ajisai pass shown in Figure 1, with the various determinations of the mean given relative to the mean obtained using 3.0 × rms rejection.

Rej.	Mean(cm)	No.Pts.
3.0 × rms	0.00	1104
2.5 × rms	0.19	1081
2.0 × rms	0.58	1030
1.5 × rms	1.18	936
1.0 × rms	1.72	799
0.5 × rms	2.13	501

The peak of the distribution, as given by the smoothing method, is about 2 cm from the initial mean, and it is seen that the successive estimates of the mean move closer to the peak as the rejection level is reduced. For the rejection level of 0.5 × rms a large number of points have been rejected, and also in tests on various passes some difficulty was experienced in obtaining convergence. So for subsequent tests we have adopted a level of 1.0 × rms.

Objections that are frequently raised to using a tight rejection level are that too much data is being discarded, and that the data are being made to look better than they really are. However what we are proposing is that this tight rejection level is used only for the purpose of obtaining an estimate of the peak of the pass distribution, so that the bias of the peak from the 3.0 × rms mean can be determined. The means in the normal point bins and the value of the rms of the whole pass will be calculated from the data that remain after making a 3.0 × rms rejection.

4.3 Pearson curves

A distribution of n points x_i with mean $\bar{x}$ is characterised to a large extent by its moments μ_2, μ_3, μ_4 where

$$\mu_j = \frac{1}{n} \sum_{i=1}^{n} (x_i - \bar{x})^j$$

The second moment is the square of the standard deviation. The following quantities are also defined:

Skewness $= \mu_3^2/\mu_2^3$ indicates deviation from symmetry, $= 0$ for symmetry about $\bar{x}$

Kurtosis $= \mu_4/\mu_2^2$ indicates degree of peakiness, $= 3$ for Gaussian distribution.

These quantities are dimensionless and of restrained magnitude, and so are in some applications more convenient than the 3rd and 4th moments. This conventional definition of skewness has the disadvantage that the sign of the 3rd moment is lost, and it is this which describes the direction of the skewness. (It may be better to define skewness as $\mu_3/\mu_2^{3/2}$.) In the plots in this paper we attach the sign of the 3rd moment to the skewness.

There is a method in statistics of deriving a distribution function from values of these three moments obtained from a set of data. These are the Pearson distributions (see description by M.G. Kendall, The Advanced Theory of Statistics, Vol 1, 1947). The distribution function f of the quantity x is defined by a differential equation

$$\frac{df}{dx} = \frac{(x-a)f}{b_0 + b_1 x + b_2 x^2}$$

where

$$a = -\mu_3(\mu_4 + 3\mu_2^2)/A$$

$$b_0 = -\mu_2(4\mu_2\mu_4 - 3\mu_3^2)/A$$

$$b_1 = -\mu_3(\mu_4 + 3\mu_2^2)/A$$

$$b_2 = -(2\mu_2\mu_4 - 3\mu_3^2 - 6\mu_2^3)/A$$

$$A = 10\mu_4\mu_2 - 18\mu_2^3 - 12\mu_3^2$$

and where the origin of x is now at its mean value. The peak of the distribution curve is at $x = a$.

This differential equation has several forms of analytical solution depending on the values of the moments. For values likely to be met in practice its solution is of the form

$$f = k(1 + \frac{x}{a_1})^{m_1}(1 - \frac{x}{a_2})^{m_2}$$

but for the precise values of the moments corresponding to a Gaussian distribution this solution becomes singular, and it has an alternative solution which is in fact the Gaussian distribution. So unfortunately the analytical solution is close to a singularity in the region likely to be met in practice, and so is not a very useful way of deriving the shape of the curve. However it is easy to solve the differential equation by numerical integration starting from the peak, although there can be problems as the singularity on the x axis is approached

which require a little fudging. Some solution curves are shown in Figure 2 for a range of values of skewness and kurtosis. No attempt has been made to normalise the area under the curves; they are all plotted with the same height at the peak. It is seen that the shapes of the curves are close to a Gaussian curve until fairly extreme values of the parameters are reached, eg., skewness of 0.6 or kurtosis of 2.2, and then the shapes are not particulary typical of what is seen in some SLR data, and so it can be expected that this method will give a good estimate of the peak for distributions close to Gaussian, but not be so useful in more extreme cases.

This discussion of how to plot the Pearson curves is given here for completeness, but it is not proposed that this should be a normal procedure for SLR data handling. However the method provides a simple estimator of the location of the peak of a distribution of data. Expressed in terms of the standard deviation σ, the skewness s, and the kurtosis k, with consideration given to the sign of the 3rd moment, the displacement of the peak from the mean is

$$a = \frac{-s^{1/2}\sigma(k+3) \times \mathrm{sign}(\mu_3)}{10k - 18 - 12s}$$

5. Comparison of methods of peak determination

Figure 3 shows the results of applying these various methods of peak determination to a number of passes tracked by RGO Herstmonceux. The passes were selected to provide a good test of the methods, and are not necessary typical passes from the station. The figures give the following information:

- the conventional histogram, using a bin of 40 ps (= 6 mm)
- the smoothing-method distribution function plotted as a solid curve
- the Pearson distribution function plotted as a dashed curve
- the 3 × rms-rejection mean shown as a solid vertical line from the top
- the 1 × rms-rejection mean shown as a dashed vertical line from the top.

The two distribution curves are plotted with slightly different peak heights for clarity, and the peak height of the histogram is limited if necesssary to be slightly below these two curves.

The information given in the captions includes:

- Smoothing parameter σ in ps (multiply by 0.15 to get mm)
- Bias(1): difference of smoothing-method peak from 3 × rms mean
- Bias(2): difference of 1 × rms mean from 3 × rms mean
- Bias(3): difference of Pearson peak from 3 × rms mean.

Figures 3(a) and 3(b) show passes with insignificant skewness, in which all methods of determining the peak and mean agree well.

Figures 3(c), 3(d) and 3(e) show passes with significant skewness, in which smoothing, Pearson and 1 × rms agree well, but are significantly different from the 3 × rms mean.

Figures 3(f) and 3(g) show passes in which smoothing and 1 × rms agree well, but the Pearson peak stands off, and all differ from the 3 × rms mean.

Figures 3(h) and 3(i) show passes in which the Pearson peak and 1 × rms agree fairly well, but the smoothing peak stands off.

From these and tests on numerous other passes we conclude that:

- for a single-photon station there is often a significant difference of the peak from the 3 × rms-rejection mean
- the 1 × rms-rejection mean usually agrees with one or other of the smoothing peak and Pearson peak, and often with both.

6. Recommendations

In conclusion we recommend the following:

a) the ranges to a calibration target or the trend-removed data from a whole satellite pass should be screened at an iterated 3 × rms level, and in the process determine *rms* and *mean* of the retained data

b) the skewness and kurtosis of the retained data should be determined

c) using this fixed value of *rms* a second determination of the mean should be made using an iterated 1 × *rms* rejection. This provides an estimate of *peak*. Then the bias of the calibration or pass is $bias = peak - mean$

d) for a calibration run, use the value of *peak* as the calibration value

e) for a satellite pass, form normal points from the screened data within each bin in the usual way, but add the correction *bias* to the normal point.

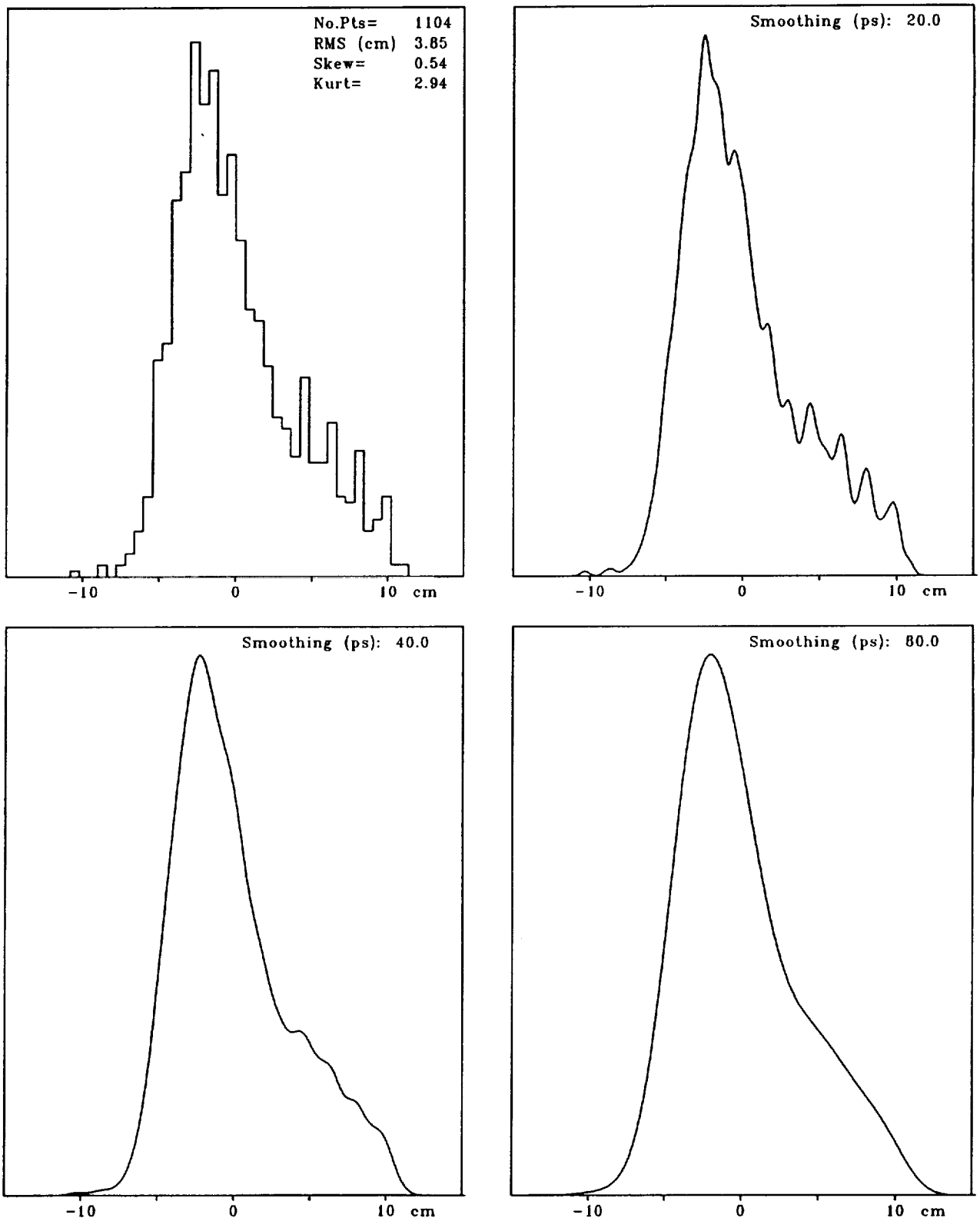

Figure 1. Use of the smoothing method to determine the distribution of an Ajisai pass.

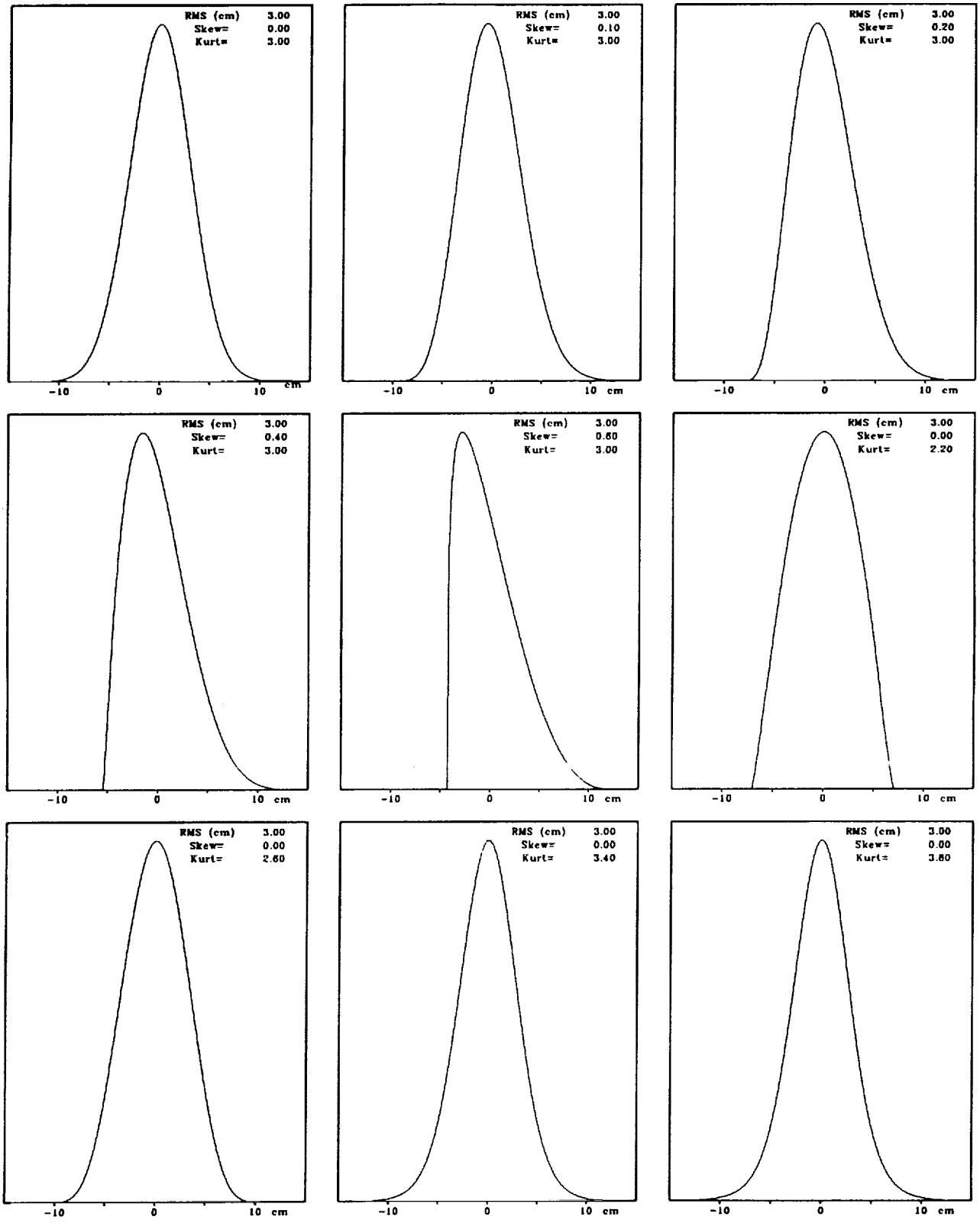

Figure 2. A range of Pearson distribution curves.

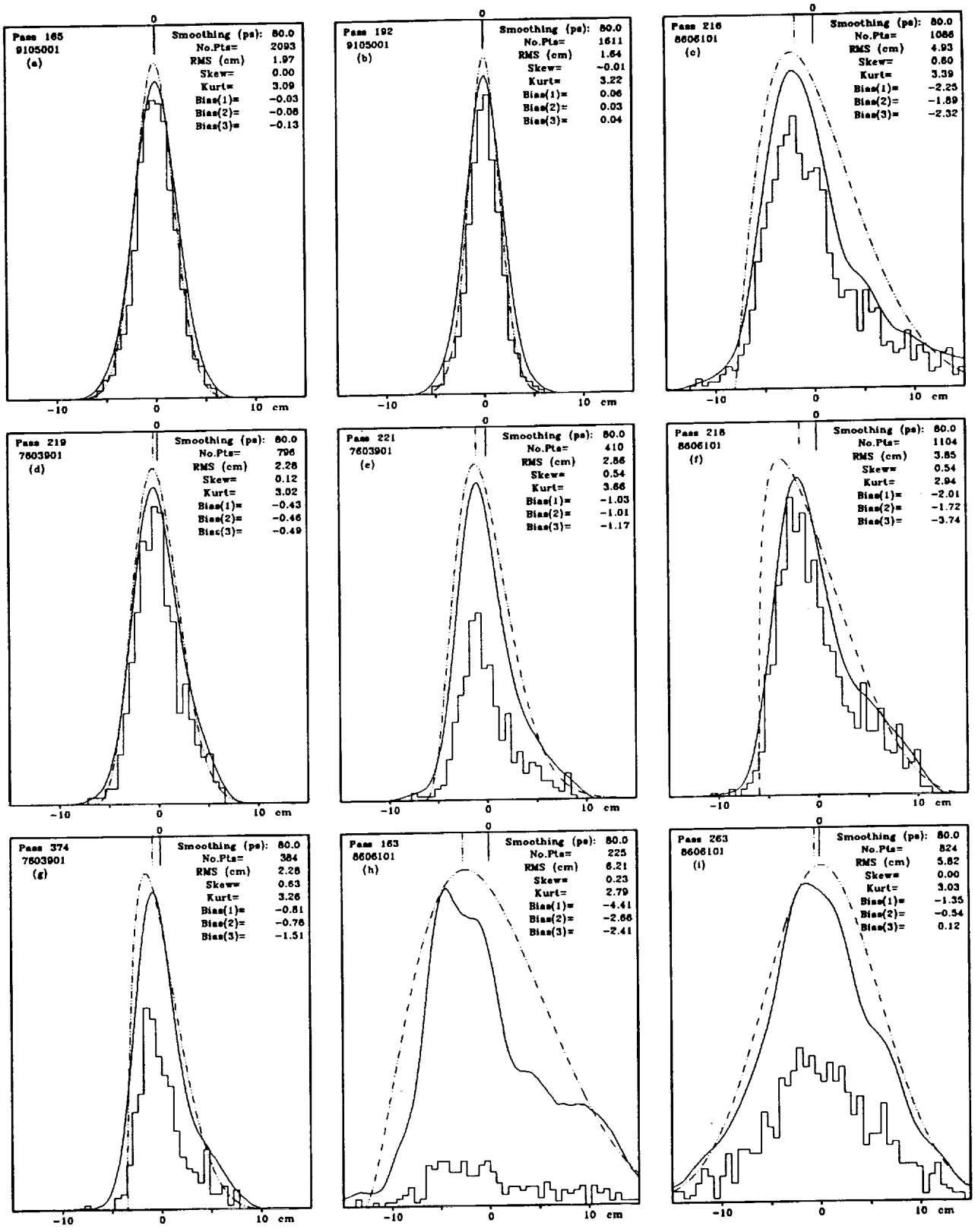

Figure 3. Comparison of methods of peak determination.

ADAPTIVE MEDIAN FILTERING FOR PREPROCESSING OF TIME SERIES MEASUREMENTS

Matti Paunonen

Finnish Geodetic Institute
Ilmalankatu 1A
SF-00240 Helsinki, Finland
Telefax:358-0-264995

ABSTRACT.

A median (L1-norm) filtering program using polynomials was developed. This program was used in automatic recycling data screening. Additionally a special adaptive program to work with asymmetric distributions was developed. Examples of adaptive median filtering of satellite laser range observations and TV satellite time measurements are given. The program proved out versatile and time saving in data screening of time series measurements.

1. INTRODUCTION

The advantages of data screening of satellite laser range measurements using median (or L1-norm) instead of least squares were shown earlier (Paunonen 1989). The median is known to be insensitive to outlying observations, which is a useful property in preliminary data screening of any time series measurements. Asymmetric distributions often arise for various reasons; saturation of the laser detector and the receiver electronics, laser prepulses etc. This cannot be easily treated with least squares methods.
In response to multiple needs, a median program permitting use of a higher order polynomial of up to ten was developed. A second version used automatic recycling of the fitting loop until a specified fit was obtained and a special program to work with unsymmetric distributions was devised. Examples of screening satellite laser range observations and TV satellite time measurements are given.

2.1 MEDIAN PROGRAM

The median program was constructed with the Fortran-procedure published by Barrodale and Roberts (1974), modified for polynomial use. The function to be minimized in the overdetermined case is

$$\sum_{1}^{M} \left| y_i - a_0 - a_1 x_i - a_2 x_i^2 - \ldots - a_N x_i^N \right| \quad , \tag{1}$$

where y_i are the observations, x_i the observing times (here), M the number of observations and N the degree of the polynomial to be fitted to the observations, and a_j (j=0...N) the coefficients of the polynomial.

2.2 AUTOMATIC MEDIAN FILTER PROGRAM

A versatile data screening program should be able to run automatically, without any manual interface. The median is good basis for a filtering program, because it selects reliably the densest part of the measurements as a reference. This means that any erratic points, that is outliers, are of true size, and not evened out as in the least squares method. Operation of the sequential median filtering program is started by forming the residuals of all the observations and calculating their average. Observations below a certain rejection limit are selected for the next cycle only. The problem is to find a suitable limit which is neither too inclusive nor too exclusive. Good operation was obtained by using the rejection level, R,

$$R = 3.5 * AVR \quad , \tag{2}$$

where AVR is the average of the residuals in the earlier round. For a Gaussian-shaped distribution the width between the zero and the point corresponding to one standard deviation is 1.46 times the width corresponding to the average. Thus the limit used is roughly equivalent to 2.4 times the standard deviation used in the least squares method. The repeated rounds are limited to four, but the final selection is generally ready after three rounds.

2.3 ADAPTIVE AUTOMATIC MEDIAN FILTER PROGRAM

In practice, the distribution of the data may be asymmetric and may include separated peaks. In satellite laser ranging, a distribution as shown in Fig.1 can easily arise with mode-locked lasers. The transmitted pulse may contain a small prepulse if selection of a single laser pulse from a train of mode-locked laser pulses is incomplete. Even if the parasitic pulse is small, it causes stops in the photon counting mode. This poses difficulties for normal screening methods using least squares. Use of only

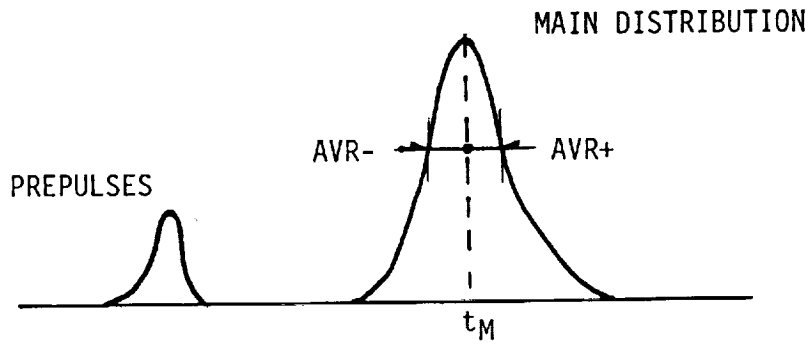

Fig. 1. An asymmetric distribution of possible range residuals in satellite laser ranging.

a two sigma-limit (Appleby and Sinclair 1991) is possible, but it may also fail if the contamination is severe. The median is expected to perform better because it finds the location of the main pulse more easily. The main part may also show unbalanced distribution (skewness) due, for instance, to saturation effects in the receiving electronics.

A modified method for asymmetric distributions is proposed as a refinement of the median filter described. Because the median produces separate average values for positive and negative residuals, AVR+ and AVR-, respectively, the program is allowed to select a minimum of the absolute values, and use it as the basis for the rejection limit in Eq.(2),

$$AVR = Min(|AVR+|, |AVR-|) \quad . \tag{3}$$

At least mild skewness will be corrected in this way. If the distribution is symmetric, operation is normal.

3. TESTS OF THE ADAPTIVE MEDIAN FILTERING

The first test set was obtained from satellite laser range observations to the distant LAGEOS- satellite at Metsähovi, Fig. 2a. This is a mixture of good and bad observations. The points on the shorter range side arose from the shape of the laser pulse (Paunonen 1989). The short 4.5 ns pulse was cut by an electro-optical shutter from a 20 ns long ruby laser pulse. However, the shutter operation was not perfect and sometimes some leakage due, for instance, to changing temperature, may have occurred. This leakage, which was less than 10 per cent, looks like a pedestal on which a short pulse is riding.

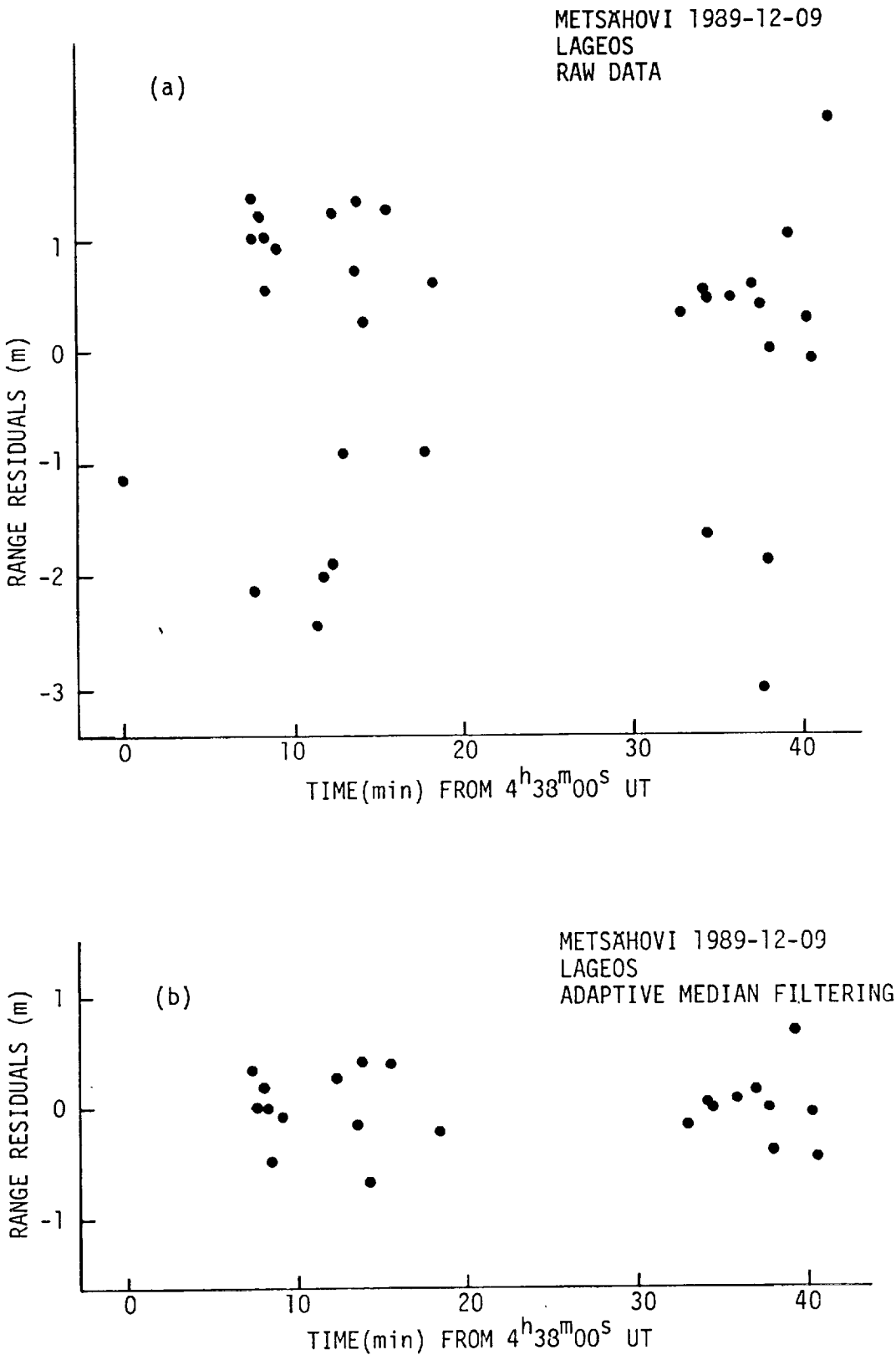

Fig. 2. a) Unscreened range residuals in a LAGEOS pass
b) Range residuals after adaptive median filtering (linear fit).

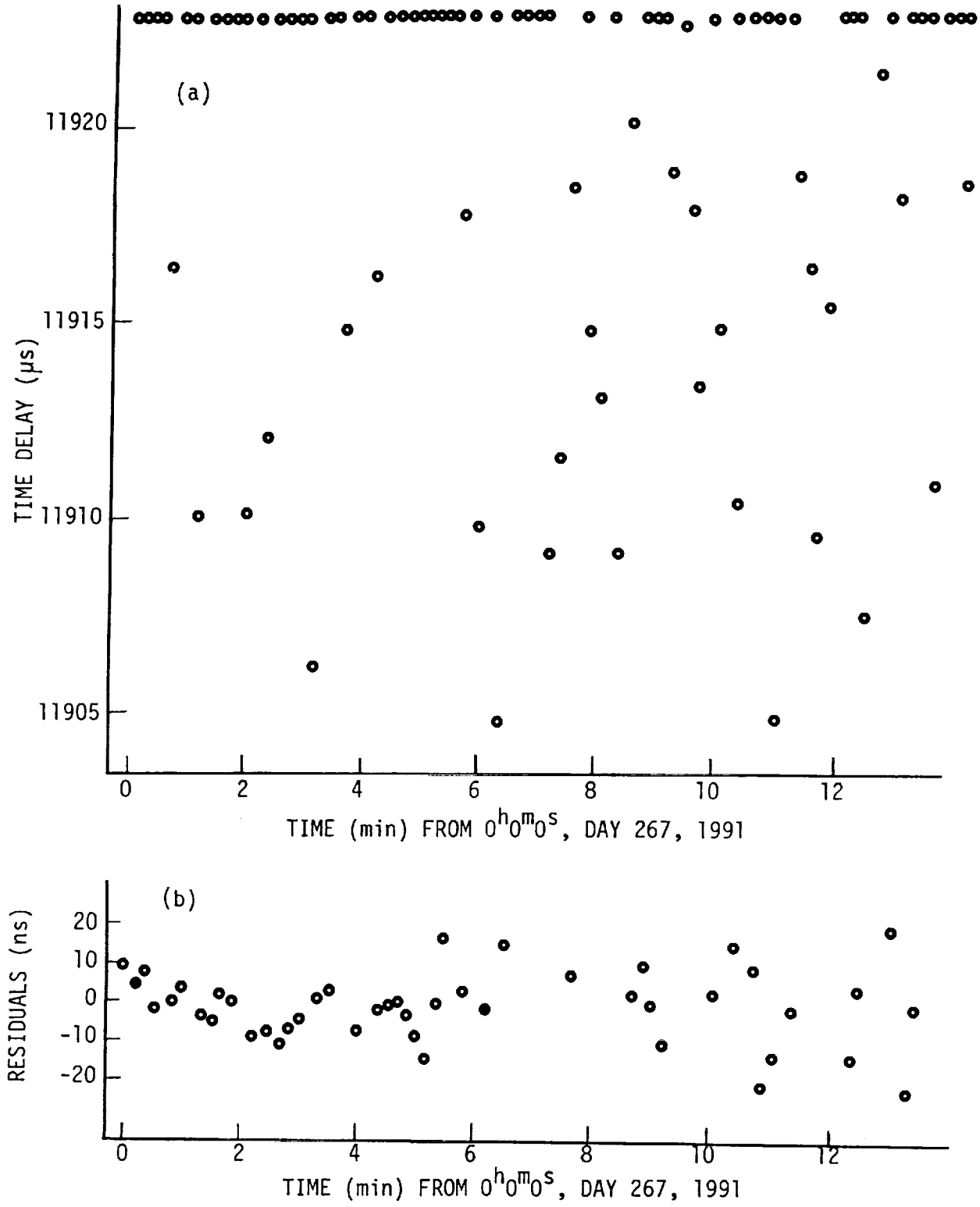

Fig. 3. a) Unscreened time measurements from a TV satellite
b) Time residuals after adaptive median filtering (parabolic fit).

The energy ahead of the main pulse may stop the time interval counter. The adaptive median filter selected 22 observations from the 33 available ones (Fig. 2b). The initial data set is not random, because similar results were also obtained at the calibration line. The result is also plausible, because its width corresponds to the laser pulse width. The earlier method for testing one observation at a time (Paunonen 1982) would be of little value, without knowing what to seek.

Another test set originated from recent TV satellite time measurements (Fig. 3a). Here the second tick from the station clock started the time interval counter and the horizontal syncronization pulse from a satellite TV receiving system (50 Hz rate) stopped it. The large number of badly timed pulses propably originated from the encrypting method the TV transmission (program RAIUNO on the EUTELSAT 1-F5 satellite) is using. This set was also cleared well with the adaptive median filter (Fig. 3b). The r.m.s. value of the residuals was 11 ns.

4. DISCUSSION AND CONCLUSIONS

The adaptive median filter has proved to be versatile and to save time. It can safely remove several outliers, however large they are. This is a big advantage over the least squares method, in which all large outliers must be removed before any useful operations can be obtained. Polynomials should be used with care also in median filtering. End points in particular may behave peculiarly. The median program sets the value of some residuals at zero (this number is same as the degree of the polynomial), which is artificial. The asymptotic estimation efficiency of median is also usually worse than that of the mean (Eadie, et.al.,1971). It seems therefore best to use the median in the data screening phase and to use the normal least squares method for final extraction of the results. Use of the least squares is then well justified, because the distribution of the screened data is nearly normal.

REFERENCES

Appleby, G.M. and A.T. Sinclair (1991). Formation of on-site normal points. Satellite Laser Ranging Newsletter, SLR Subcommission of the CSTG (International Coordination of Space Techniques for Geodesy and Geodynamics), April 1991, pp. 25-28.

Barrodale, I. and F.D.K. Roberts (1974). Solution of an overdetermined system of equations in the l1 norm. Communications of the ACM, Vol. 17, No. 6, pp. 319-320.

Eadie, W.T., D. Dryard, F.E. James, M. Roos, B. Sadoulet (1971). Statistical Methods in Experimental Physics. North-Holland Publishing Company, Amsterdam 1971, 296 pp.

Paunonen, M. (1982). Studies on the Metsähovi satellite laser ranging system. Reports of the Finnish Geodetic Institute, 1982:2, Helsinki 1982, 47 pp.

Paunonen, M. (1989). Use of the L1-norm in screening laser range observations to satellites. Proc. of the 18th INTERKOSMOS Symposium on the Use of Artificial Satellite Observations for Geodesy and Geophysics, June 12-17, 1989, Cracow, Poland, (Ed. WL. Goral, Polish Academy of Sciences, Observations of Artificial Satellites of the Earth, No 27, Warsaw 1990), pp. 359-362.

SATCOP MISSION PLANNING SOFTWARE PACKAGE

S. BUCEY
Bendix Field Engineering Corp.
Seabrook, MD

New laser ranging capabilities, additional satellites, and changing priorities are making it more difficult to determine the most efficient method of operations for NASA's CDSLR Network. A software package called SATCOP (Satellite Ranging Coordination Programs) has been developed to assist in mission support and planning operations. Its uses range from planning daily station operations to conducting pre-launch satellite visibility studies. SATCOP provides a listing and graphics output of satellite visibility for a given occupation site for any time period. SATCOP may also be used to determine the optimum ranging scenario for a station, taking into account satellite ranging priorities and station operational requirements. Finally, SATCOP may be used to illustrate simultaneous satellite visibility for multiple stations.

Introduction

As the CDSLR Network grows into the 1990's it is undergoing many changes in both its capabilities and requirements. On the one hand great progress has been made in terms of increasing the SLR systems' performance. Upgrades to the onsite computer and improved laser ranging hardware have greatly increased the number of satellite passes which can be acquired during an operating shift by reducing the amount of time needed for operations other than actual ranging. On the other hand, more requirements have been placed on the systems. Many more satellites have become available, with more scheduled for launch, thus increasing the likelihood of simultaneous satellite visibility. In addition, the possible scenarios required for ranging these many satellites are changing frequently, with conflicting priorities and needs.

It became apparent that some tools needed to be developed to assist the planners in determining Network ranging priorities. Such tools have been developed at Bendix under the direction of NASA's Dynamics of the Solid Earth Project (DOSE) for both long range planning and routine operations to maximize the amount of data collected. This paper will review some of these tools and describe their uses.

The SATCOP software package has several parts which are used for both routine operations and pre-launch scheduling. The use of such software helps determine pre-mission requirements such as ground track determination, forecasted station performance, predictions of optimum system locations, and predicted satellite visibility. SATCOP also produces graphs of ground tracks of acquired passes; determines availability of simultaneous ranging opportunities; schedules operating hours for maximum visibility; and produces automated single station scheduling for daily station activities.

Figure 1 is a time plot of satellite visibility for a given station. This figure demonstrates that even with just 6 satellites considered the opportunities for laser ranging are abundant. Such plots, and others like it, are used for operational scheduling of station activities and for the determination of operational requirements for future missions or locations. Typically such a plot is done for a 7 day period, but the number of satellites and number of days is user determined. The plot consists of a time scale in hours GMT across the top, and a day scale down the left. A subscale of each day is present, dividing each day into a line for each satellite. For each satellite, a two letter satellite identifier indicates the horizontal line across which the satellite could be visible (refer to Figure 8 to identify the satellite associated with each two letter identifier). Across the plot a solid line indicates when a satellite is visible, and a total number of minutes for that day is printed on the right. On the last day of the plot a column on the right also indicates the total number of minutes visible during the time period of the plot.

Figure 2 illustrates the number of possible sightings of two satellites over a four day period at 5 locations. Such graphs are used when extended time periods are considered, and can be used to compare satellite visibility at several stations simultaneously. Such graphs are useful for determining the best of several possible station locations and the expected visibility at a given location, and can include several satellites. Often it is also desired to know the number of possible simultaneous sightings of a satellite for several locations. Figures 3 and 4 demonstrate the tools used for determining this number. Figure 3 is a matrix showing the number of mutual sightings possible at several locations. The number of such sightings for a given pair of stations is found by cross indexing between the two desired stations to find the result within the matrix; as an example for MOBLAS 4 (7110) and MOBLAS 8 (7109) the number of such sightings is found to be 130. Figure 4 is a listing of all possible subsets of the desired stations which can range, along with the times of mutual availability. The user can determine the minimum number of stations desired for simultaneous ranging, and the time period for consideration.

The SATCOP software package has been developed to provide support for other purposes as well. Figure 5 is a plot which shows the distribution of acquired LAGEOS passes reported as quicklook data for the time period May 2 to May 14, 1992. This type of plot allows the user to quickly

determine the geographic distribution of data reported during the indicated time period. Figure 6 is used to compare sightings for two or more stations over a 24 hour period, and is read similarly to Figure 1. Such a graph is convenient for quickly determining the opportunities for coordinated activities between two or more locations with one or more satellites.

A major use for the SATCOP package is single station scheduling for daily activities. The purpose of such scheduling is to assist the station crew in conducting laser operations by considering as many of the requirements and opportunities presented to the station as possible, and then producing a schedule which is a possible 'optimum' solution for the day's activities.

To perform such scheduling many parameters are considered. A major requirement is to resolve ranging opportunities when two or more satellites are visible simultaneously. SATCOP considers satellite priority, ranging limitations such as a maximum time limit on a satellite pass, and day or night ranging restrictions. If two satellites of the same priority are available then the software ensures that ranging is as evenly distributed between the two during the day as possible, based on available minutes of data. Activities which may exclude laser activities are taken into account, such as data preprossessing and calibration time. If the system has the multi-satellite calibration capability then the software determines a best sequence for calibration and ranging.

As an example a schedule generated for MOBLAS 4 at Monument Peak will be considered, using the time period covered by Figure 1. Some of the parameters used for generating the schedule are illustrated in Figures 7 and 8. As an aid to readability only two days will be scheduled, but normally a regular workweek is considered. The hours of operation were determined previously using other methods described earlier. From this information the schedule sent to the station is graphically shown in Figure 9. Looking at the plot for each day there is a line corresponding to each satellite plus an additional line showing laser calibration, denoted by 'C1'. Since this system is using the multi-satellite calibration capability data may be acquired on several satellites between calibrations. Also, since the overhead time has been greatly reduced by this, and other, upgrades true interleaving of passes is possible when a high priority short pass occurs at the same time as a low priority long pass. The thick line represents the time that the station is actually ranging (or calibrating), while the thin line represents the time the satellite is actually visible (the thick line corresponding to the ranging of a given pass is located above the thin line).

Conclusion

In the future the requirements for SLR activities will only become greater. New satellites, new ranging scenarios, and new station abilities will require changes to be made to the methods used to schedule operations. Recent examples are the ETALON campaign and the multi-

satellite upgrade. Of course, many possible parameters have yet to be considered. Obviously it is impossible to account for poor weather conditions deterring laser activities on a given day, but plans are being considered to include long term weather effects as a statistical modification of the predicted station performance. And it would be similarly difficult to account for system down time due to component failure. But the use of this package, and its continued improvement, has allowed Bendix to more efficiently coordinate the NASA CDSLR network activities.

SATELLITE VISIBILITY: mobl4 (MT PEAK)

FIGURE 1

9/18/92 – 9/19/92

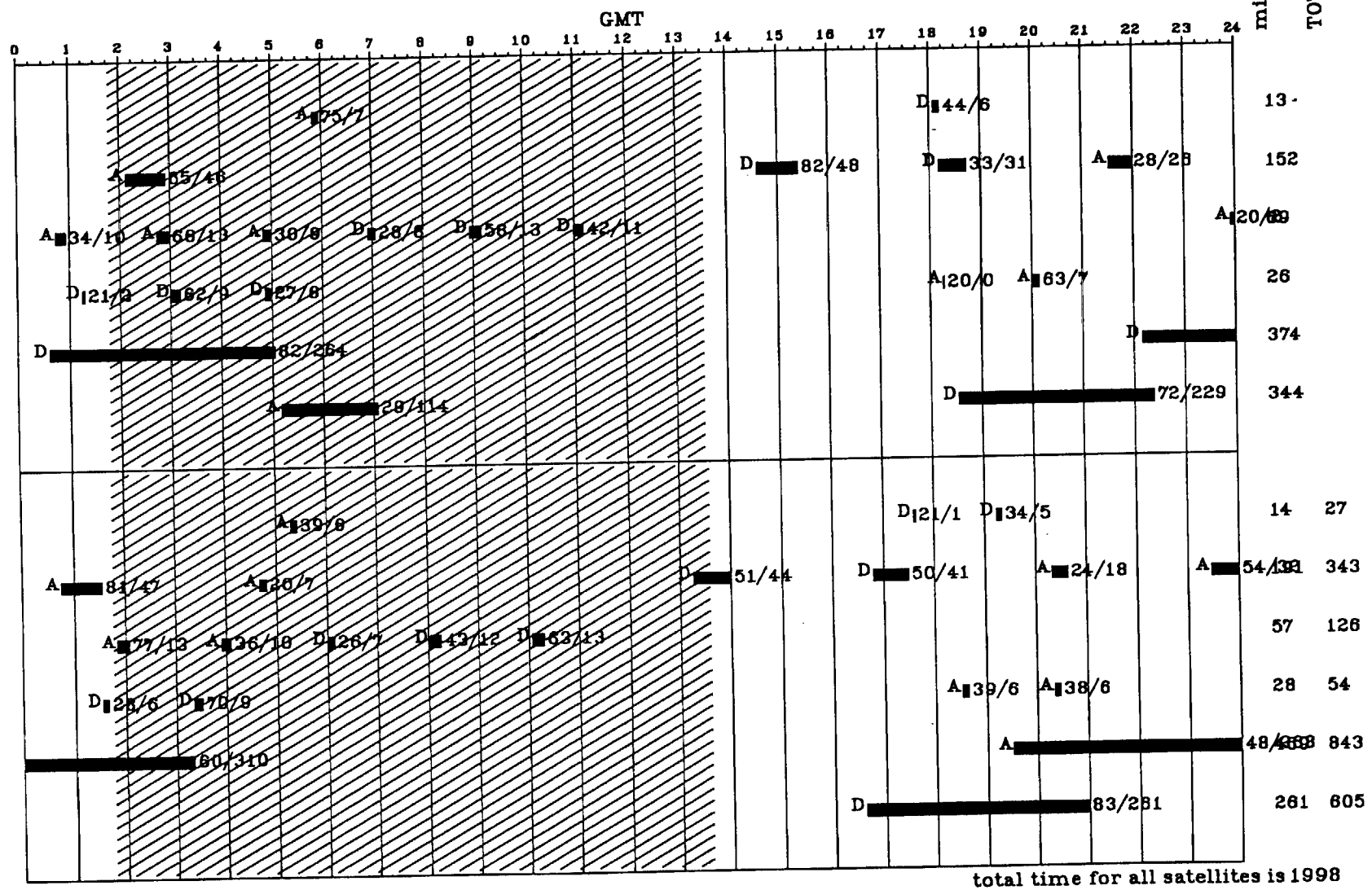

date created: 9/15/92

CDSLR/OAS

BUCEY

letter on curve indicates ascending/descending

SHADED SECTION IS NIGHT

NOTATION ON PASS IS MAXIMUM ELEVATION–

AND NUMBER OF MINUTES

PASSES BY STATION AND SATELLITE

FIGURE 2

	511 517		518 524		525 531		601 607			Totals	
7110	LAG	AJI	LAG	AJI	LAG	AJI	LAG	AJI		LAG	AJI
DAY	15	0	11	4	15	8	12	16			
TWILIGHT	2	0	4	2	1	3	1	2		137	161
NIGHT	18	40	19	35	19	28	20	23			
7090	LAG	AJI	LAG	AJI	LAG	AJI	LAG	AJI		LAG	AJI
DAY	15	9	15	16	15	19	12	23			
TWILIGHT	1	2	0	2	1	0	1	3		130	150
NIGHT	17	27	18	20	15	18	20	11			
7105	LAG	AJI	LAG	AJI	LAG	AJI	LAG	AJI		LAG	AJI
DAY	14	3	12	9	13	15	11	21			
TWILIGHT	2	2	2	2	1	2	1	3		127	138
NIGHT	16	30	18	23	18	18	19	10			
7109	LAG	AJI	LAG	AJI	LAG	AJI	LAG	AJI		LAG	AJI
DAY	14	0	11	1	15	6	12	14			
TWILIGHT	3	0	3	2	1	3	1	2		134	152
NIGHT	17	38	19	35	18	28	20	23			
7080	LAG	AJI	LAG	AJI	LAG	AJI	LAG	AJI		LAG	AJI
DAY	17	5	13	10	16	18	14	22			
TWILIGHT	3	3	3	2	1	2	1	3		159	205
NIGHT	20	43	24	39	23	32	24	26			

Mutual sightings of LAGEOS by any two stations FIGURE 3
for the period 920511.0 to 920607.0

The upper diagonal is number of mutual trackings.
The lower diagonal is minutes of mutual trackings.

	7080	7090	7105	7109	7110	7112	7123	7210	7843	7939
7080	0	0	119	130	133	0	52	81	0	14
7090	0	0	0	0	0	0	0	0	113	0
7105	3326	0	0	105	106	0	0	18	0	60
7109	5109	0	1997	0	130	0	45	77	0	0
7110	4719	0	1847	4337	0	0	45	74	0	0
7112	0	0	0	0	0	0	0	0	0	0
7123	1057	0	0	420	521	0	0	70	38	0
7210	2369	0	74	1908	1788	0	1431	0	14	0
7843	0	2783	0	0	0	0	668	54	0	0
7939	168	0	413	0	0	0	0	0	0	0

****

FIGURE 4

these 4 stations can track on the sighting date 920511
during the common sighting time 00:20:10.00 to 00:34:43.00
7110 00:05:52.00 to 00:34:43.00 start az: 15. ang: 20. end az:296. ang: 20. max el: 31.
7109 00:01:34.00 to 00:39:16.00 start az: 27. ang: 20. end az:278. ang: 20. max el: 44.
7080 23:48:34.00 to 00:40:56.00 start az: 40. ang: 0. end az:291. ang: 0. max el: 24.
7210 00:20:10.00 to 01:02:15.00 start az: 10. ang: 20. end az:243. ang: 20. max el: 52.

---

these 2 stations can track on the sighting date 920511
during the common sighting time 01:14:01.00 to 01:50:09.00
7843 01:01:28.00 to 01:50:09.00 start az: 31. ang: 20. end az:207. ang: 20. max el: 87.
7090 01:14:01.00 to 01:52:20.00 start az: 84. ang: 20. end az:192. ang: 20. max el: 43.

---

these 4 stations can track on the sighting date 920511
during the common sighting time 03:23:43.00 to 03:43:45.00
7105 03:06:19.00 to 03:43:45.00 start az:125. ang: 30. end az:337. ang: 30. max el: 73.
7110 03:23:23.00 to 03:51:47.00 start az: 63. ang: 20. end az:346. ang: 20. max el: 31.
7109 03:23:43.00 to 03:58:34.00 start az: 69. ang: 20. end az:331. ang: 20. max el: 39.
7080 03:01:36.00 to 04:00:45.00 start az: 98. ang: 0. end az:331. ang: 0. max el: 36.

---

these 5 stations can track on the sighting date 920511
during the common sighting time 06:59:19.00 to 07:06:41.00
7105 06:52:48.00 to 07:06:41.00 start az:239. ang: 30. end az:283. ang: 30. max el: 33.
7210 06:59:19.00 to 07:23:26.00 start az: 71. ang: 20. end az: 13. ang: 20. max el: 27.
7110 06:39:10.00 to 07:27:03.00 start az:146. ang: 20. end az:334. ang: 20. max el: 87.
7109 06:43:49.00 to 07:31:46.00 start az:145. ang: 20. end az:333. ang: 20. max el: 89.
7080 06:24:30.00 to 07:33:54.00 start az:158. ang: 0. end az:336. ang: 0. max el: 74.

Figure 5

QUICK-LOOK ANALYSIS REPORT

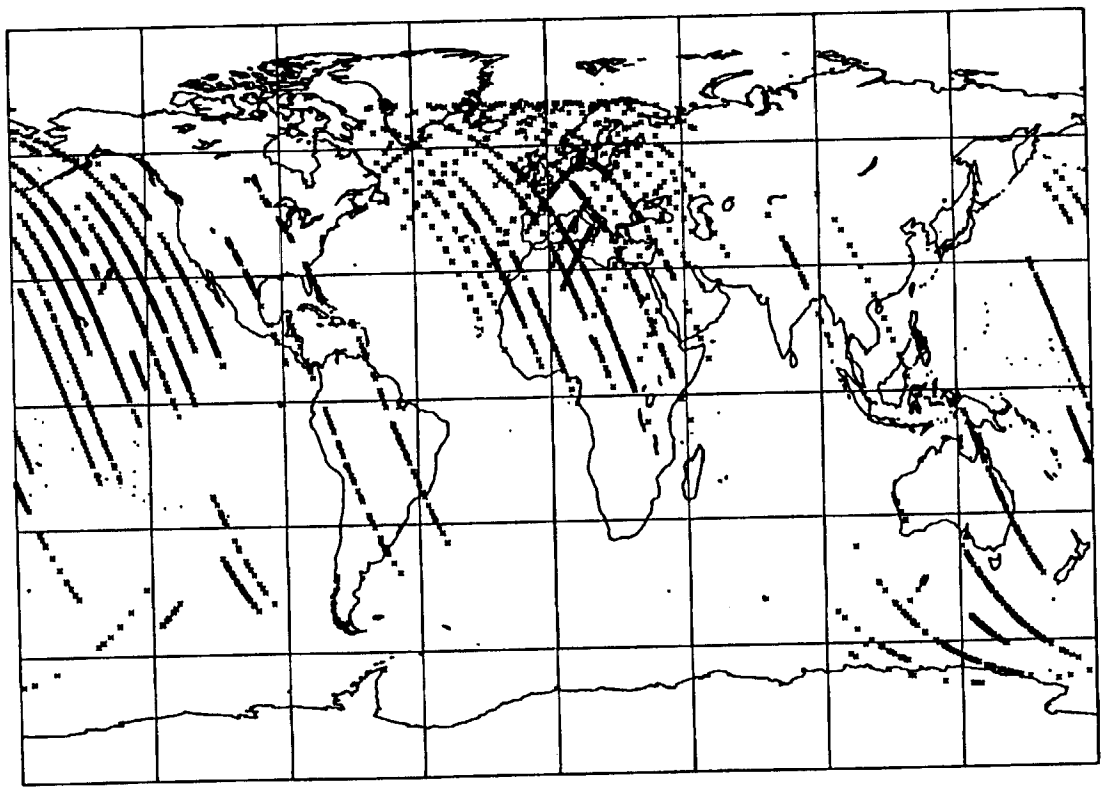

AUG 1 - AUG 7 1992

ALLIED-SIGNAL AEROSPACE/BENDIX FIELD ENGINEERING CORP. CDSLR/DSG/OAS

SATELLITE VISIBILITY: 92/ 9/14

FIGURE 6

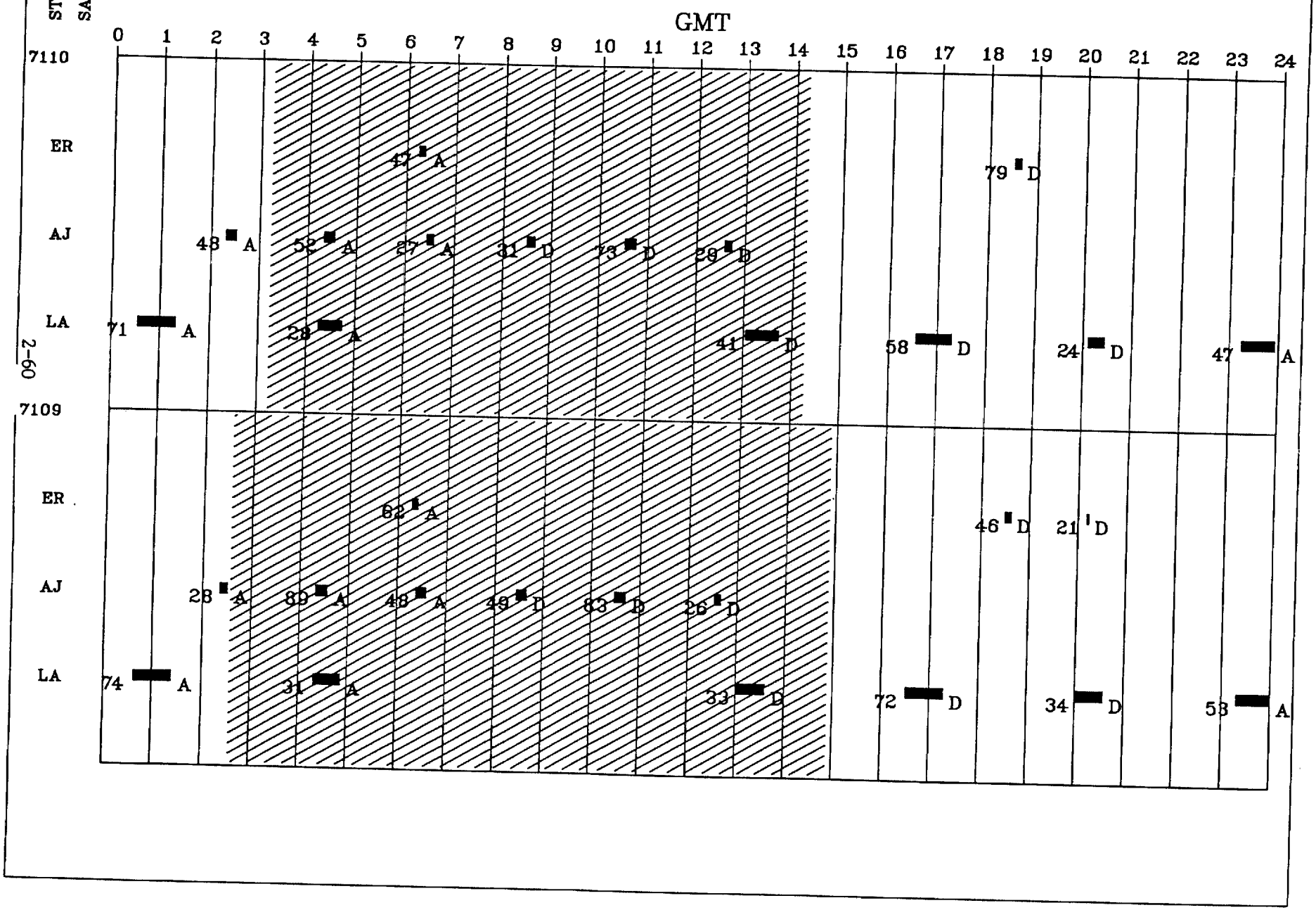

FIGURE 7

SYSTEM TRACKING PARAMETERS FOR MOBLAS 4 AT MT. PEAK.

1. MAY TRACK BOTH DAY AND NIGHT.
2. REQUIRES ABOUT 7 MINUTES FOR PRE/POST-PASS EXTERNAL CALIBRATION.
3. MINIMUM TRACKING ANGLE IS 20 DEG.
4. SYSTEM ABLE TO PROCESS ACQUIRED DATA IN PARALLEL WITH OTHER OPERATIONS.
5. SYSTEM USING MULTI-SATELLITE CALIBRATION CAPABILITY.
6. THE SATELLITE PRIORITIES, MINIMUM TRACK AND OTHER PARAMETERS ARE CHOSEN FOR DEMONSTRATION BUT MAY VARY WITH SATELLITE AND STATION.

FIGURE 8

SATCOP INPUT PARAMETERS

1. TRACKING PERIOD: SEP 18 - SEP 19, 1992.

2. STATION AVAILABILITY: 24 HOURS/DAY.

3. "WORK WEEK": 2 DAYS.

4. SATELLITE PRIORITIES:
   1: ERS-1 (E1 OR ER)
   2: LAGEOS (L1 OR LA)
   3: AJISAI (AJ)
   4: STARLETT (ST)
   5: ETALON 1 (MT)
   5: ETALON 2 (NT)

NOTE: ETALON TRACKING LIMITED TO 45 MINUTE SEGMENTS.

SATELLITE VISIBILITY: MOBL4 (7110)
9/18/92 – 9/19/92 SHIFT NUMBER 1

FIGURE 9

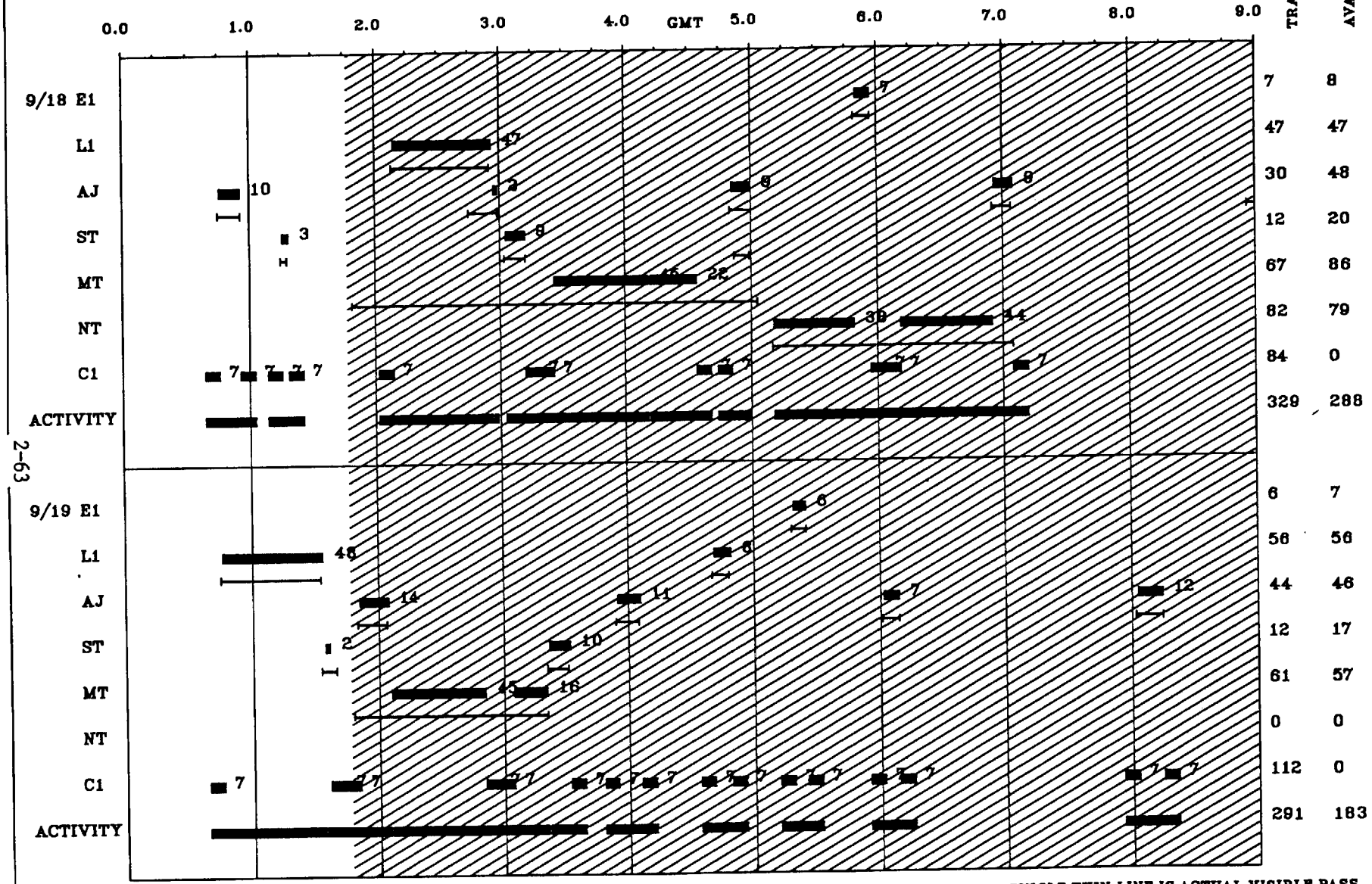

date created: 9/15/92
BFEC/CDSLR DSG Bucey
Conklin

THICK SOLID CURVE IS ACTUAL TRACKING.
ATTACHED THIN CURVE IS PRE/POST CAL TIMES.
NOTATION ON PASS IS MINUTES OF PASS TRACKED.

SINGLE THIN LINE IS ACTUAL VISIBLE PASS.

SHADED SECTION IS NIGHT.